Cellular and Molecular Life Sciences (2023) 80:324
https://doi.org/10.1007/s00018-023-04974-7

ORIGINAL ARTICLE

Macrophage neogenin deficiency exacerbates myocardial remodeling and inflammation after acute myocardial infarction through JAK1-STAT1 signaling

Jishou Zhang[1,2] · Yao Xu[2] · Cheng Wei[2] · Zheng Yin[2] · Wei Pan[2] · Mengmeng Zhao[2] · Wen Ding[2,4] · Shuwan Xu[2] · Jianfang Liu[2] · Junping Yu[2] · Jing Ye[2] · Di Ye[2] · Juan-Juan Qin[1,3] · Jun Wan[1,2] · Menglong Wang[1,2]

Received: 20 February 2023 / Revised: 1 September 2023 / Accepted: 20 September 2023 / Published online: 12 October 2023

Abstract

Immune response plays a crucial role in post-myocardial infarction (MI) myocardial remodeling. Neogenin (Neo1), a multifunctional transmembrane receptor, plays a critical role in the immune response; however, whether Neo1 participates in pathological myocardial remodeling after MI is unclear. Our study found that Neo1 expression changed significantly after MI in vivo and after LPS + IFN-γ stimulation in bone marrow-derived macrophages (BMDMs) in vitro. Neo1 functional deficiency (using a neutralizing antibody) and macrophage-specific Neo1 deficiency (induced by $Neo1^{flox/flox}$;$Cx3cr1^{cre}$ mice) increased infarction size, enhanced cardiac fibrosis and cardiomyocyte apoptosis, and exacerbated left ventricular dysfunction post-MI in mice. Mechanistically, Neo1 deficiency promoted macrophage infiltration into the ischemic myocardium and transformation to a proinflammatory phenotype, subsequently exacerbating the inflammatory response and impairing inflammation resolution post-MI. Neo1 deficiency regulated macrophage phenotype and function, possibly through the JAK1-STAT1 pathway, as confirmed in BMDMs in vitro. Blocking the JAK1-STAT1 pathway with fludarabine phosphate abolished the impact of Neo1 on macrophage phenotype and function, inflammatory response, inflammation resolution, cardiomyocyte apoptosis, cardiac fibrosis, infarction size and cardiac function. In conclusion, Neo1 deficiency aggravates inflammation and left ventricular remodeling post-MI by modulating macrophage phenotypes and functions via the JAK1-STAT1 signaling pathway. These findings highlight the anti-inflammatory potential of Neo1, offering new perspectives for therapeutic targets in MI treatment.

Jishou Zhang, Yao Xu and Cheng Wei have contributed equally to this work.

✉ Juan-Juan Qin
qinjuanjuan@whu.edu.cn

✉ Jun Wan
wanjun@whu.edu.cn

✉ Menglong Wang
whuwangmenglong@163.com

[1] Department of Cardiology, Renmin Hospital of Wuhan University, Department of Geriatrics, Zhongnan Hospital of Wuhan University, Wuhan University, 238 Jiefang Road, Wuhan 430060, China

[2] Department of Cardiology, Renmin Hospital of Wuhan University, Hubei Key Laboratory of Cardiology, Cardiovascular Research Institute, Wuhan University, Wuhan, China

[3] Center for Healthy Aging, Wuhan University School of Nursing, Wuhan, China

[4] Department of Radiology, the First Affiliated Hospital, Zhejiang University School of Medicine, Hangzhou, China

Graphical abstract

Neo1 deficiency aggravated inflammation and left ventricular remodeling after MI by modulating macrophage phenotypes and functions via the JAK1-STAT1 signaling pathway.

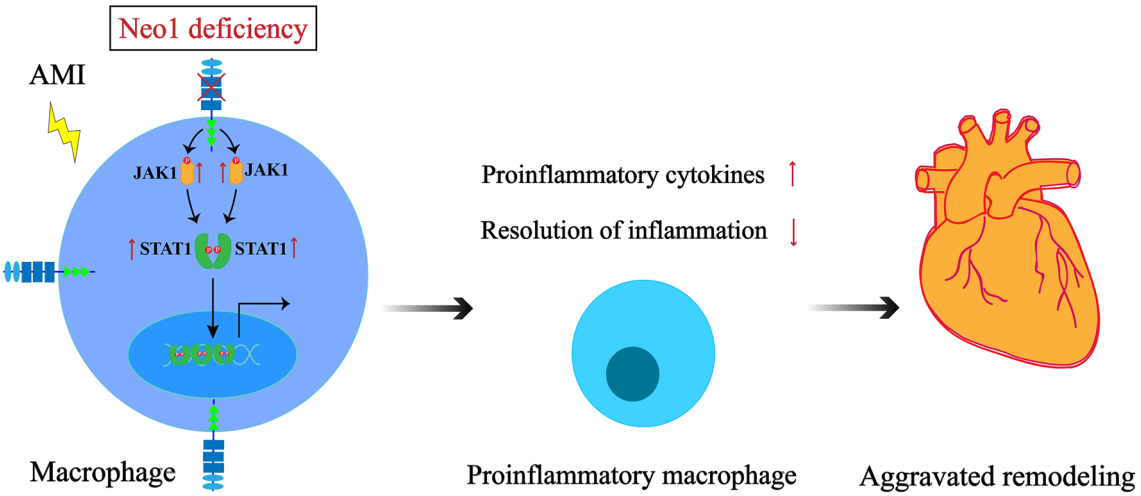

Keywords Neogenin · Myocardial infarction · Proinflammatory macrophage · Inflammation resolution

Abbreviations

BMDMs	Bone marrow-derived macrophages
Flu	Fludarabine phosphate
MI	Myocardial infarction
JAK1	Janus kinase 1
Neo1	Neogenin
STAT1	Signal transduction and activator of transcription 1

Introduction

Myocardial infarction (MI) is irreversible cardiomyocyte necrosis caused by sudden hypoxia and ischemia in the heart. Pathological myocardial remodeling after MI contributes to several adverse events, such as malignant arrhythmia, heart failure and sudden death, which affect the prognosis of patients with MI [1, 2]. The inflammation triggered by MI contributes to pathological myocardial remodeling, during which several immune cells are activated and a large number of cytokines are produced in cardiac tissue [3]. For example, monocytes quickly invade after MI, with the Ly6C^{high} monocytes predominating in the early stage (the first 3 days) and Ly6C^{low} monocytes exhibiting remarkable tissue repair function in the late phase (between 4 and 7th day after MI) [4]. Several studies have revealed that inhibiting excessive inflammation and promoting inflammation resolution have beneficial effects on myocardial remodeling after MI [5, 6]. The CANTOS clinical trials showed that anti-inflammatory therapy targeting interleukin-1β (IL-1β) with canakinumab could further reduce the risk of recurrent cardiovascular events in patients with previous MI based on standard pharmaceutical therapy [7], directly indicating that anti-inflammatory therapy could improve the prognosis of MI patients and that inflammation may play an important role in myocardial remodeling after MI. Therefore, it is imperative to further explore inflammatory mechanisms and identify critical targets for regulating the inflammatory response in myocardial remodeling after MI, which will contribute to the treatment of patients with MI.

In the early stage of MI, the microenvironment promotes a proinflammatory macrophage phenotype (M1 macrophages), which contributes to the secretion of a large number of cytokines [8]. The excessive maintenance of proinflammatory macrophages leads to the deterioration of cardiac function and myocardial remodeling. Inhibiting proinflammatory macrophages or increasing reparative macrophages in different ways exerted a protective effect on myocardial remodeling after MI [9, 10]. Li et al. [10] revealed that the ablation of hypoxia-induced mitogenic factors could attenuate myocardial remodeling after MI by promoting macrophage transformation to the reparative phenotype. A decrease in M1 macrophages induced by dectin1 depletion could lead to improvements in myocardial remodeling and cardiac

function [11]. Therefore, macrophages play a critical role in myocardial remodeling after MI, and identifying a novel target to regulate macrophage function is necessary in the treatment of myocardial remodeling after MI.

Neogenin (Neo1), a multifunctional transmembrane receptor, belongs to the immunoglobulin (Ig) superfamily. Neo1 contains one extracellular domain that consists of 4 immunoglobulin-like regions and 6 fibrin FNIII functional regions, one transmembrane region and one intracellular domain and is the receptor of netrin1 and repulsive guidance molecules (RGMs) [12, 13]. In the nervous system, Neo1 is associated with several pathophysiological processes, such as nerve development, axon guidance and the regulation of neuronal activity [14–16]. In addition, studies suggest that Neo1 can regulate inflammation in several inflammatory diseases, such as autoimmune encephalitis, peritonitis and hepatic ischemia–reperfusion injury [17–19]. Neo1 is expressed in human macrophages, and Neo1 inhibition could increase macrophage efferocytosis of apoptotic neutrophils, promoting inflammation resolution and tissue regeneration [20]. In neuromyelitis optica, RGMs could increase the expression of CXCL2 by binding to Neo1 in macrophages, inducing neutrophil infiltration and inflammatory reactions [21]. These results suggest that Neo1 plays a critical role in macrophage function and that targeting Neo1 may be a promising strategy to regulate inflammation and myocardial remodeling after MI. Therefore, in this study, we explored the regulatory effect of Neo1 on the macrophage phenotype and myocardial remodeling after MI.

Materials and methods

Animals

WT C57BL/6 mice (male, aged 8–10 weeks old, 23–25 g) were purchased from Gempharmatech Co., Ltd. (Nanjing, China). $Cx3cr1^{cre}$ mice and $Neo1^{flox/flox}$ ($Neo1^{F/F}$) mice were obtained from Cyagen Biosciences (Suzhou, China) and Gempharmatech Co., Ltd., respectively, and were used to generate macrophage-specific Neo1 knockout mice, $Neo1^{F/F}$;$Cx3cr1^{cre}$ mice. Both $Cx3cr1^{cre}$ mice and $Neo1^{F/F}$ mice have a C57BL/6 background. Spleen macrophages were stained with $CD45^{+}CD11b^{+}F4/80^{+}$ and obtained with fluorescence-activated cell sorting. Then spleen macrophages were processed to extract RNA and to perform reverse transcription and RT-qPCR. The results verified that Neo1 was specifically knocked down in macrophages in $Neo1^{F/F}$;$Cx3cr1^{cre}$ mice (Fig. S1a and b**).** All mice were maintained at the Cardiovascular Research Institute of Wuhan University in a standard laboratory environment (70% relative humidity, 22 °C, 12:12-h (h) light–dark cycle). In this study, all animal experiments were performed in accordance with the principles of blinding and randomization, and all efforts were made to minimize animal suffering. All animal experiments complied with the guidelines of directive 2010/63/EU of the European Parliament and were approved by the Animal Care and Use Committee of Renmin Hospital of Wuhan University (WDRM20181215), Wuhan, China.

MI surgery

After being acclimatized to the new environment for 1 week, WT, $Neo1^{F/F}$ and $Neo1^{F/F}$;$Cx3cr1^{cre}$ mice underwent MI surgery by permanent ligation of the left anterior descending (LAD) coronary artery, as described with minor modifications [22, 23]. In brief, after the mice were anesthetized using pentobarbital sodium (50 mg/kg, intraperitoneal injection) and underwent thoracotomy, the proximal LAD artery was encircled and ligated by a 7–0 proline suture. The LAD artery in the sham group was encircled but not ligated. At different time points after MI, echocardiography was performed, the mice were euthanized by CO_2 inhalation, and cardiac tissue was obtained for further analysis.

Functionality deficiency of Neo1 in animals

To implement the functionality deficiency of Neo1 in WT C57BL/6 mice, mice were administered a Neo1 neutralizing antibody (anti-Neo1) or IgG control (2 μg per mouse, dissolved in PBS, intravenous injection (i.v.)) 2 h before MI or sham surgery and subsequently once per week after surgery. The dose of Anti-Neo1 and dosage regimen were determined by previous studies [20, 24] and were verified by a preexperiment in our study. Both goat Anti-Neo1 (#AF1079) and goat IgG control (#AB-108-C) were purchased from R&D Systems (Minnesota, USA).

Bone marrow-derived macrophage (BMDM) isolation and culture

BMDMs were obtained from C57BL/6 J mice, as described previously [25]. In brief, after C57BL/6 J mice (8–10 weeks, male) were euthanized and sterilized, the tibias and femurs were isolated. Then, the marrow cavity was exposed and washed with RPMI 1640 medium, and the cell suspension was obtained. After the cell suspension underwent filtration (a 70 μm strainer), erythrocyte lysis (using a red blood cell lysis buffer (Servicebio, China) for 3 min) and washing, the target bone marrow cells were resuspended in 10% FBS (in RPMI 1640 medium with 1% penicillin/streptomycin). Then, macrophage colony-stimulating factor (M-CSF, 20 ng/ml) was used for one week to allow BMDM differentiation. The differentiated BMDMs were treated with LPS (100 ng/ml) and IFN-γ (10 ng/ml) to induce a proinflammatory

phenotype, and the sham group was treated with PBS. Anti-Neo1 or IgG (5 μg/ml) [20] was administered 0.5 h before stimulation with LPS and IFN-γ. After stimulation for 12 h, the cultured cells were used for further analysis. LPS (#L2880) was purchased from Sigma (USA). M-CSF (#315–02-10) and IFN-γ (#315–05-20) were obtained from Peprotech (Rocky Hill, USA).

To overexpress Neo1 in BMDMs, adenoviral vectors of Neo1 (Ad-Neo1, purchased from Hanbio, Shanghai, China) were added to the culture medium of BMDMs. After 48 h of Ad-Neo1 supplementation, LPS and IFN-γ were administered to stimulate BMDMs for 12 h.

Blockade of the STAT1 signaling pathway by fludarabine phosphate (Flu)

Flu (#A8317, APExBIO, USA) was used to block STAT1 signaling pathway activation. In mice, Flu was administered via intraperitoneal injection at a dose of 100 mg/kg (dissolved in 90% PBS + 10% DMSO, 1 day before MI and every other day from day 1 to day 21 after MI) [26, 27]. In BMDMs, Flu (100 μM) [28] was added to the culture medium 1 h before stimulation with LPS and IFN-γ.

Echocardiography

Echocardiography was performed on the mice as described previously [29]. After the mice were anesthetized with 1.5% isoflurane, left ventricular function was evaluated by a VINNO 6 device (VINNO Technology Co., Ltd, Suzhou, China) with a linear probe working at a frequency of 23 MHz. The analyzed items included heart rate, left ventricular end diameter in diastole (LVEDd), left ventricular end diameter in systole (LVEDs), left ventricular ejection fraction (LVEF) and left ventricular fraction shortening (LVFS).

Triphenyl tetrazolium chloride (TTC) staining

Hearts were isolated 3 d after MI and stored at − 20 °C for 30 min [30]. Then, hearts were sectioned into 3 mm short axis slices that were immediately incubated with TTC solution at 37 °C for 30 min in the dark and subsequently fixed with 4% paraformaldehyde. The infarction size was calculated as the percentage of infarction area (white)/the whole area of the heart.

Real-time qPCR (RT–qPCR)

RNA was extracted from the cardiac infarction border [31] tissue of mice by TRIzol reagent [29] (Invitrogen Life Technologies, USA). A Transcriptor First Strand cDNA Synthesis kit (Roche, Germany) was used to synthesize cDNA, and LightCycler 480 SYBR Green Master Mix (Roche, Germany) was used for subsequent PCR amplification. The human qPCR primers included Neo1 and GAPDH. The mouse primers included Neo1, atrial natriuretic peptide (ANP), brain natriuretic peptide (BNP), collagen I, collagen III, serum tumor necrosis factor α (TNF-α), interleukin (IL)-1β, IL-6, monocyte chemoattractant protein-1 (MCP-1), and GAPDH. All primers are shown in Table S1.

Western blotting

Protein was extracted with RIPA buffer from the cardiac infarction border tissue of mice and BMDMs and further separated as described previously [29]. Primary antibodies included: Neo1 (R&D system), collagen I (Servicebio), Bax (Abcam), Bcl-2 (Abcam), cleaved-caspase3 (GeneTex), phospho (p)/total (T)-P38 (CST), p/T-ERK (CST), p/T-JNK (CST), p-janus kinase 1 (JAK1) (CST), T-JAK1 (Abcam), p-JAK2 (CST), T-JAK2 (Abcam), p-signal transduction and activator of transcription 1 (STAT1) (Abcam), T-STAT1 (CST), p/T-P65 (Abcam), p/T-STAT6 (CST), GAPDH (GeneTex), Chemerin receptor 23 (ChemR23) (Santa Cruz), formyl-peptide receptor-2 (FPR2) (Santa Cruz), and G protein-coupled receptor 37 (GPR37) (Santa Cruz). Then, the blots were incubated with a secondary antibody (goat anti-rabbit antibody or rabbit anti-mouse antibody; CST, Boston, USA).

Flow cytometry analysis

For cardiac tissue of mice, flow cytometry was used as described in our previous study [32]. In brief, left ventricular tissue was digested with 0.1% collagenase II and 2.4 U/ml dispase II for 30 min to prepare a single-cell suspension that was subsequently filtered with a 70 μm strainer and managed with red blood cell lysate (Servicebio, China) for 3 min. Then, anti-CD16/32 antibody (BD Biosciences) was used to block Fcγ receptors, and Fixable Viability Stain 510 (BD Biosciences) was used to separate viable and nonviable cells. Finally, for cell surface markers, primary antibodies were used for flow cytometry, including anti-CD11b (PE-cy7, eBioscience), anti-F4/80 (APC, eBioscience), anti-Ly6C (Bv605, BD Biosciences), anti-CD86 (Bv421, BD Biosciences), and anti-MerTk (PE, eBioscience). After the primary antibodies were incubated for 30 min in the dark, the cells were analyzed with CytExpert (Beckman, USA) or MoFlo XDP (Beckman, USA). The gating strategy: cardiac macrophages, $CD11b^{+}F4/80^{+}$; cardiac proinflammatory macrophages, $CD11b^{+}F4/80^{+}Ly6C^{high}$ (Fig. S2a) or $CD11b^{+}F4/80^{+}Ly6C^{high}CD86^{+}$ (Fig. S2b); cardiac proresolving macrophages, $CD11b^{+}F4/80^{+}Ly6C^{low}MerTk^{+}$ (Fig. S2c).

To detect neutrophils phagocytized by macrophages and analyze the ratio of neutrophils associated with macrophages to total neutrophils, primary antibodies against CD11b, Ly6G (Bv421, BD Biosciences) and F4/80 were used to label cell surface markers for 30 min. Then, the cell suspension underwent fixation and permeabilization. After that, Ly6G antibody was used to label the neutrophils phagocytized by macrophages. The ratio of neutrophils associated with macrophages ($CD11b^+Ly6G^+F4/80^+$) to total neutrophils ($CD11b^+Ly6G^+$) was used to evaluate macrophage efferocytosis for apoptotic neutrophils (Fig. S2d).

In mice, the spleen was ground and subsequently filtered with a 70 μm strainer to prepare a single-cell suspension. After splitting with red blood cell lysate, the cell suspension was managed using anti-CD16/32 antibody and fixable viability stain 510. Then, several primary antibodies were used for flow cytometry, including anti-CD45 (APC-Cy7, BD Biosciences), anti-CD11b and anti-Ly6C. The gating strategy: spleen monocytes, $CD45^+CD11b^+$ or $CD11b^+$; spleen proinflammatory monocytes, $CD45^+CD11b^+$ $Ly6C^{high}$ or $CD11b + Ly6C^{high}$.

For BMDMs, cells in culture dishes were digested with 0.25% trypsin to prepare BMDM suspensions. Then, anti-CD16/32 antibodies (BD Biosciences) were used to block Fcγ receptors, and Fixable Viability Stain 510 (BD Biosciences) was used to separate viable and nonviable cells. The primary antibodies included anti-F4/80 and anti-CD86. The gating strategy: proinflammatory BMDM, $F4/80^+CD86^+$.

Flow cytometric sorting and splenic macrophage extraction

A single-cell suspension of spleen was generated as described above. Then, the cell suspension was managed using anti-CD16/32 antibody and fixable viability stain 510. Primary antibodies, including anti-CD45, anti-CD11b and anti-F4/80, were used to sort and obtain spleen macrophages that subsequently were used to perform RNA extraction, reverse transcription and QT-qPCR, analyzing whether Neo1 was specifically deleted in macrophages from mice.

Untargeted lipidomics

For sample preparation and lipid extraction, lipids were extracted according to the MTBE method. Briefly, the left ventricular tissue (50 mg) was spiked with appropriate amounts of internal lipid standards and homogenized by an MP homogenizer. Then, the mixture underwent MTBE administration, ultrasound and sitting. After that, the mixture was centrifuged, and the upper layer solution was obtained and dried under nitrogen. The lipid extracts were redissolved in 90% isopropanol/acetonitrile and centrifuged at 14,000 × g for 15 min, and 3 μL of the upper layer was injected.

For untargeted lipidomics analysis, the extracts were analyzed by LC−MS at Shanghai Applied Protein Technology Co., Ltd. In brief, lipids were separated on a Waters ACQUITY PREMIER CSH C18 Column (1.7 μm, 2.1*100 mm) under the following chromatographic conditions: mobile phase A (acetonitrile:water = 6:4, v/v) and mobile phase B (acetonitrile:isopropanol = 1:9, v/v) at a flow rate of 300 μL/min and column oven temperature at 45 °C. The gradient started with 30% of B and was held for 2 min. Then, the gradient was increased to 100% of B over 23 min, which was returned to 30% B over 1 min and was finally equilibrated for 9 min. To avoid the influence of signal fluctuation, a random injection sequence was used for analysis of samples.

Then, MS detection was performed using a Thermo Scientific™ Q Exactive mass spectrometer equipped with an ESI (Electron Spray Ionization) ion source. Data were acquired in both positive and negative ion modes. Data-dependent acquisition methods were used for MS/MS analyses of the lipidome. Finally, LipidSearch 4.0 software was used for peak detection and annotation of lipids or internal standards. For statistical analysis, lipids with significant differences were identified based on a combination of statistically significant thresholds of variable influence on projection (VIP > 1) values obtained from the orthogonal partial least squares discriminant analysis (OPLS-DA) model (multidimensional statistical analysis) and two-tailed Student's t test ($P < 0.05$).

Hematoxylin–eosin (HE), Masson and picrosirius red (PSR)

Hearts were fixed with 4% paraformaldehyde for 3 days and subsequently embedded in paraffin. Hearts on the short axis (papillary level) were sliced into 5 μm sections that were stained with HE, Masson and PSR as described previously [33]. Based on HE and Masson staining, infarction size was calculated as total infarct circumference divided by total LV circumference × 100, as described previously [34]. Based on PSR staining, fibrosis was calculated as the total fibrosis area divided by the total area of LV tissue. These data were measured and calculated using ImageJ software (National Institutes of Health, Bethesda, USA).

Immunofluorescence

These sections were used to perform immunofluorescence (IF), as described in our previous study [35]. The primary

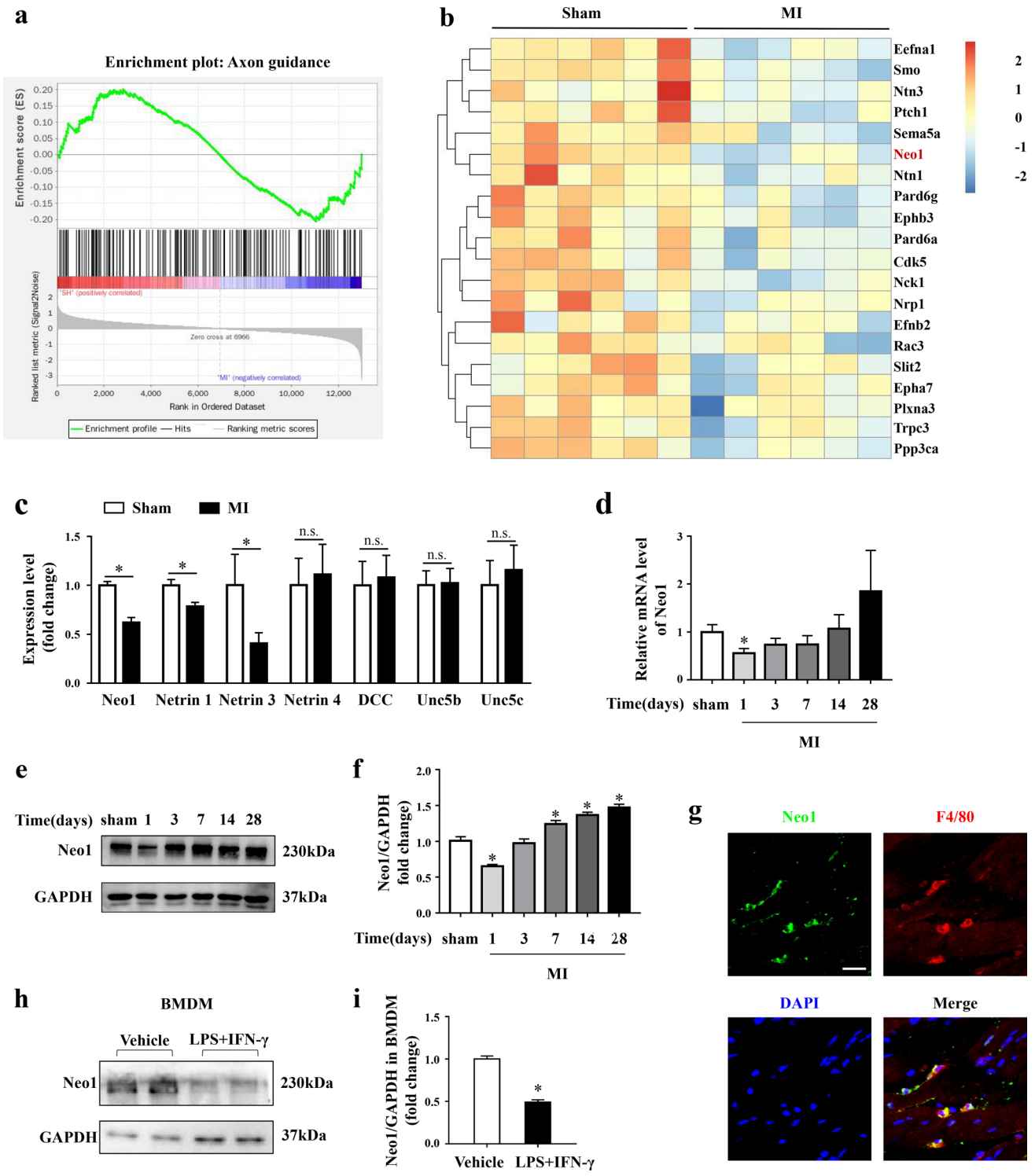

antibodies included cleaved-caspase3 (GeneTex), Neo1 (R&D), F4/80 (Servicebio), CD86 (ServiceBio), inducible nitric oxide synthase (i-NOS) (CST), CD206 (R&D), Ly6G (Servicebio), p-STAT1 (Abcam), p-P65 (Abcam) and p-STAT6 (CST). After being incubated with primary antibodies overnight at 4 °C, the sections were incubated with the appropriate secondary antibodies for 1 h at 37 °C. The nuclei were stained with 4,6-diamidino-2-phenylindole (DAPI). Images were obtained using a fluorescence microscope (Olympus Dx51, Japan) or a confocal laser scanning microscope (Leica, Germany).

◂**Fig. 1** Neogenin (Neo1) expression in the left ventricular tissue and macrophages, The gene expression profiles of left ventricular tissue in mice challenged with MI and sham operation were downloaded from the Gene Expression Omnibus (GEO) database within the series GSE71906 and data were analyzed and shown in (**a**–**c**). **a** Gene set enrichment analysis (GSEA) enrichment plot of the Axon guidance signaling pathway in Sham vs. MI (8 h) group, n = 6; **b** Heatmap of the top 20 core-enriched genes with differential expression in the Axon guidance signaling pathway, n = 6, the included genes have the absolute values of log2 (fold change) ≥ 1.5 and adjusted p value ≤ 0.05; **c** The expression levels of Neo1, Netrin1, Netrin3, Netrin4, DCC, Unc5b and Unc5c were shown in histogram, n = 6, unpaired Student's t-test was used; **d** The mRNA levels of Neo1 at cardiac infarction border zone in mice at different time points, n = 4, one way analysis of variance (ANOVA) followed by Tukey's test; **e**, **f** The protein bands and levels of Neo1 at cardiac infarction border zone in mice at different time points, n = 4, one way ANOVA followed by Tukey's test; **g** Double-labelling immunofluorescence showed that Neo1 was expressed in F4/80^{+} macrophages in heart after MI, n = 4 in each group; **h**, **i** In bone marrow derived-macrophages (BMDMs), lipopolysaccharide (LPS) and IFN-γ were used to induced the proinflammatory phenotype of macrophages, and Neo1 expression was evaluated in vehicle and proinflammatory BMDM groups 12 h after LPS + IFN-γ stimulation, n = 4 in each group, unpaired Student's t-test. Data are expressed as the mean ± SEM. In (**c**) *indicates $p < 0.05$; In **d** and **f**, *$p < 0.05$ vs. Sham group; In **i**, *$p < 0.05$ vs. Vehicle group

TdT-mediated dUTP nick-end-labeling (TUNEL) assay

To determine cardiomyocyte apoptosis, TUNEL staining was performed with a TUNEL kit (Millipore, USA) according to the manufacturer's instructions, as described previously [35]. cTnI staining was performed using cTnI antibody (Servicebio). Images were obtained using a fluorescence microscope (Olympus Dx51, Japan).

Measurement of TNF-α and IL-1β

Serum was obtained from the mice on day 3 after MI. The serum levels of TNF-α and IL-1β were measured using enzyme-linked immunosorbent assay (ELISA) kits (Neobioscience, China) according to the instructions.

Pathway enrichment analysis

Gene expression profiles of left ventricular tissue in mice challenged with MI and sham operation were downloaded from the Gene Expression Omnibus (GEO) database within the series GSE71906. Using the microarray approach, the series provided mRNA expression data from C57BL/6 mouse hearts subjected to ligation of the left anterior descending coronary artery or sham operation, and hearts were obtained 8 h after surgery. A total of 12 samples in the series were recorded, of which 6 were from MI hearts and 6 were from sham hearts. Gene set reannotation was performed with the R package AnnoProbe version 0.1.6. In brief, to identify the Axon guidance signaling pathway, gene set enrichment analysis (GSEA) (http://www.broadinstitute.org/gsea) was performed using GSEA software 4.2.3 (Broad Institute) and visualized as a heatmap using the R package pheatmap. Genes in each gene set were obtained from the Molecular Signatures Database (MSigDB) version 7.5.1 (https://www.gsea-msigdb.org/gsea/msigdb) [36, 37].

Statistical analysis

All data are expressed as the mean ± standard error of the mean (SEM) and analyzed by GraphPad Prism 7 software. Differences between two groups were analyzed by unpaired Student's t test. Differences among the four groups were analyzed by two-way analysis of variance (ANOVA) followed by Tukey's test or one-way ANOVA followed by Tukey's test. To determine the expression of Neo1 in mice at different points after MI, differences among groups were analyzed by one-way ANOVA followed by Tukey's test. Significance was assumed to be $p < 0.05$.

Results

Neo1 expression in the left ventricular tissue and macrophages

We first performed gene set enrichment analysis using the published genotyping array datasets of the left ventricular tissue in mice 8 h after MI and sham operation. The source data are available in Gene Expression Omnibus (GSE 71906). Then, the axon guidance signaling pathway was enriched and analyzed (Fig. 1a and b) since it has a strong ability to regulate inflammation [38, 39]. In the axon guidance signaling pathway, we found that Neo1 was the top gene of core enrichment. Compared to the control group, Neo1 expression was significantly decreased in the MI group (Fig. 1b and c). In addition, Netrin1 and Netrin3 were also significantly decreased in the MI group (Fig. 1b and c). Since Neo1 is a shared receptor for Netrin1 and Netrin3 [40], the function of Neo1 in MI was regarded as the research emphasis in our study. Then, to clarify the association between Neo1 and MI, Neo1 expression was further measured by RT–qPCR and western blotting in the infarction border zone of mice at different time points. The results (Fig. 1d–f) revealed that Neo1 expression was significantly decreased 1 d after MI and gradually increased during the subsequent period (3 d, 7 d, 14 d, 28 d). A previous study suggested that Neo1 is expressed in human macrophages [20]. In our study, we demonstrated that Neo1 was expressed in macrophages in the hearts of mice after MI (Fig. 1g). In addition, in LPS- and IFN-γ-induced proinflammatory macrophages, Neo1 expression was significantly decreased

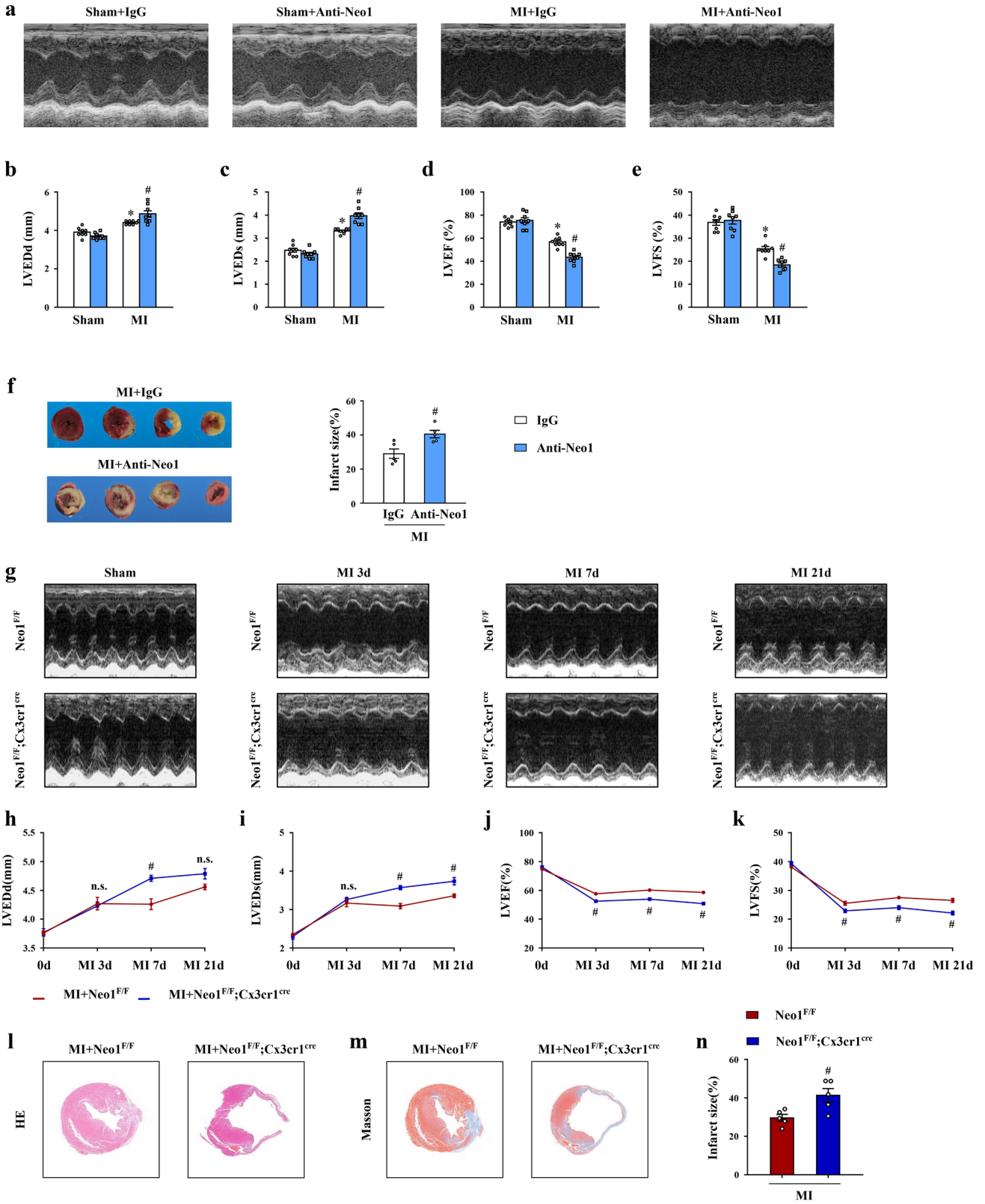
a
Sham+IgG
Sham+Anti-Neo1
MI+IgG
MI+Anti-Neo1
b
LVEDd (mm)
Sham
MI
c
LVEDs (mm)
Sham
MI
d
LVEF (%)
Sham
MI
e
LVFS (%)
Sham
MI
f
MI+IgG
MI+Anti-Neo1
Infarct size(%)
IgG
Anti-Neo1
MI
IgG
Anti-Neo1
g
Sham
MI 3d
MI 7d
MI 21d
Neo1F/F
Neo1F/F;Cx3cr1cre
h
LVEDd(mm)
n.s.
0d
MI 3d
MI 7d
MI 21d
i
LVEDs(mm)
n.s.
0d
MI 3d
MI 7d
MI 21d
j
LVEF(%)
0d
MI 3d
MI 7d
MI 21d
k
LVFS(%)
0d
MI 3d
MI 7d
MI 21d
MI+Neo1F/F
MI+Neo1F/F;Cx3cr1cre
l
MI+Neo1F/F
MI+Neo1F/F;Cx3cr1cre
HE
m
MI+Neo1F/F
MI+Neo1F/F;Cx3cr1cre
Masson
n
Neo1F/F
Neo1F/F;Cx3cr1cre
Infarct size(%)
MI

◂**Fig. 2** Macrophage neogenin (Neo1) deficiency exacerbated cardiac dysfunction and increased infarction size in mice challenged with myocardial infarction (MI), **a–e** The left ventricular (LV) function in different groups 21 days after MI, including LV end diameter in diastole (LVEDd), LV end diameter in systole (LVEDs), LV ejection fraction (LVEF) and LV faction shortening (LVFS), was evaluated by Echocardiography, n = 8 in each group, two way analysis of variance (ANOVA) followed by Tukey's test; **f** The infarction size was evaluated by triphenyl tetrazolium chloride (TTC) staining 3 days after MI, n = 5 in each group, unpaired Student's t-test; **g–k** The LV function in MI + Neo1$^{F/F}$ and MI + Neo1$^{F/F}$;Cx3cr1^{cre} groups at different time points after MI, n = 10, unpaired Student's t-test at different time points; **l–n** Based on HE staining and Masson staining 21 days after MI, infarction size was analyzed in MI + Neo1$^{F/F}$ and MI + Neo1$^{F/F}$;Cx3cr1^{cre} groups, n = 5, unpaired Student's t-test. Data are expressed as the mean ± SEM. In (**b–f**) *p < 0.05 vs. Sham + IgG group, #p < 0.05 vs. MI + IgG group; in (h–k) and (**n**), #p < 0.05 vs. MI + Neo1$^{F/F}$ group; n.s. indicates no significance

(Fig. 1h and i). Therefore, Neo1 may play a critical role in myocardial remodeling after MI by mediating macrophages.

Macrophage Neo1 deficiency exacerbated MI-induced cardiac dysfunction and increased infarction size

First, Anti-Neo1 was used to implement Neo1 functionality deficiency. Cardiac function was evaluated by echocardiography at day 21 after MI, including heart rate, LVEDd, LVEDs, LVEF and LVFS. Echocardiography showed that compared to that in the MI + IgG group, the administration of Anti-Neo1 further increased LVEDd and LVEDs and decreased LVEF and LVFS (Fig. 2a–e), indicating that Neo1 deficiency could exacerbate cardiac dysfunction after MI. No significant differences in heart rate were observed among these groups (Fig. S3a). TTC staining showed that the infarction size was significantly larger in the MI + Anti-Neo1 group than in the MI + IgG group (Fig. 2f).

To evaluate the effect of macrophage Neo1 on MI in mice, mice with macrophage-specific Neo1 deficiency, which were generated by Neo1$^{F/F}$ mice and Cx3cr1^{cre} mice, were used. Cardiac function was evaluated by echocardiography at multiple time points (day 0 (before MI), day 3, day 7 and day 21) after MI. The results showed that compared to that in the MI + Neo1$^{F/F}$ group, LVEDd was significantly increased in the MI + Neo1$^{F/F}$;Cx3cr1^{cre} group at day 7 after MI, and LVEDs were increased in the MI + Neo1$^{F/F}$;Cx3cr1^{cre} group at day 7 and 21 after MI (Fig. 2g–i). Both LVEF and LVFS were significantly lower in the MI + Neo1$^{F/F}$;Cx3cr1^{cre} group than in the MI + Neo$^{F/F}$ group at day 3, 7 and 21(Fig. 2j and k). No significant differences in heart rate were observed between the two groups at different time points (Fig. S3b). Therefore, macrophage-specific Neo1 deficiency could dramatically exacerbate left ventricular dysfunction after MI. In addition, HE and Masson staining found that the infarction size was significantly higher in the MI + Neo1$^{F/F}$;Cx3cr1^{cre} group than in the MI + Neo1$^{F/F}$ group (Fig. 2l–n). In summary, Neo1 deficiency could effectively exacerbate cardiac dysfunction and increase infarction size after MI.

Macrophage Neo1 deficiency enhanced cardiomyocyte apoptosis and cardiac fibrosis after MI

PSR staining showed that in the context of cardiac fibrosis, Anti-Neo1 could increase the cardiac fibrosis area in mice 21 days after MI (Fig. 3a and b). The mRNA expression levels of collagen I and III were significantly higher in the MI + Anti-Neo1 group than in the MI + IgG group (Fig. 3c and d). Western blotting also demonstrated that Anti-Neo1 could enhance the expression levels of collagen I after MI (Fig. S4a). In addition, the mRNA levels of ANP and BNP were also evaluated, and the results showed that Anti-Neo1 significantly increased ANP and BNP expression (Fig. S4b and c). Cardiomyocyte apoptosis was evaluated by western blotting and IF analysis. The results showed that MI increased the expression of Bax and cleaved-caspase3 and decreased Bcl-2 expression, and these changes were significantly enhanced by the administration of Anti-Neo1 (Fig. 3e–i). In addition, the TUNEL assay showed that the number of TUNEL-positive cells was significantly increased by the administration of Anti-Neo1 (Fig. 3j and k). These results indicated that functionality deficiency of Neo1 could significantly exacerbate MI-induced cardiac fibrosis and cardiomyocyte apoptosis.

Similarly, PSR staining showed that compared to that in the MI + Neo1$^{F/F}$ group, the cardiac fibrosis area was significantly increased in the MI + Neo1$^{F/F}$;Cx3cr1^{cre} group (Fig. 3l and m). For cardiomyocyte apoptosis, western blotting found that Bax expression was significantly higher and Bcl-2 expression was lower in the MI + Neo1$^{F/F}$;Cx3cr1^{cre} group than in the MI + Neo1$^{F/F}$ group (Fig. 3n and o). Double IF staining of TUNEL and cTnI also found that the number of TUNEL-positive cardiomyocytes was higher in the MI + Neo1$^{F/F}$;Cx3cr1^{cre} group than in the MI + Neo1$^{F/F}$ group (Fig. 3p and q). These results indicated that macrophage-specific Neo1 deficiency could effectively enhance cardiac fibrosis and cardiomyocyte apoptosis.

Macrophage Neo1 deficiency promoted macrophage infiltration and transformation to a proinflammatory phenotype

The infiltration and polarization of macrophages were first evaluated by flow cytometry. Our study showed that compared to that in the MI + IgG group, CD11b^{+}F4/80^{+} macrophages were significantly increased in the heart in the MI + Anti-Neo1 group 3 days after MI (Fig. 4a–c). MCP-1 plays key roles in attracting macrophages to the infarcted

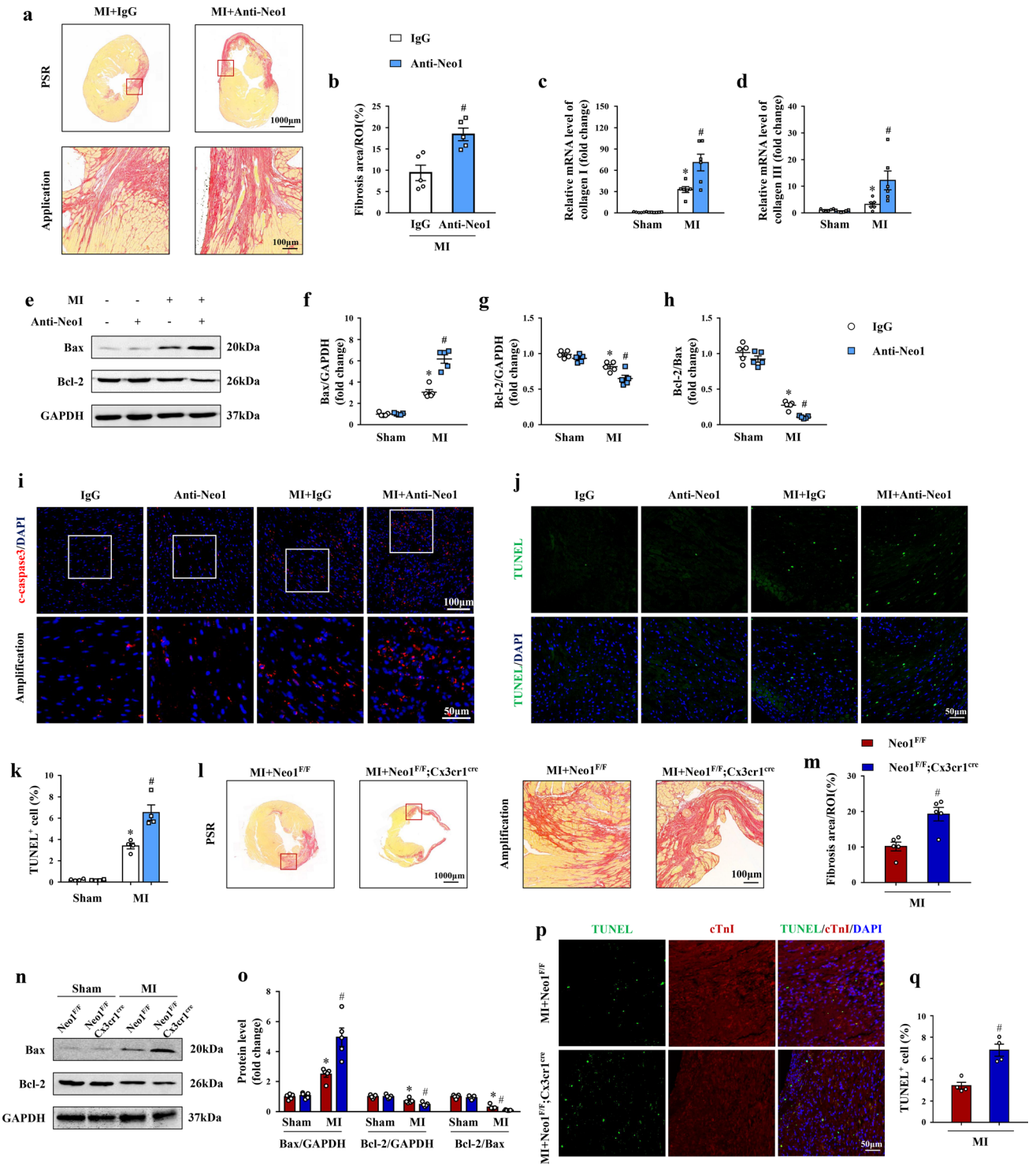

myocardium. In our study, along with the infiltration of macrophages, the expression levels of MCP-1 were increased in the MI + IgG group and were further enhanced by treatment with Anti-Neo1 (Fig. S5a). The infiltrated macrophages in the infarcted myocardium after MI could be supplemented by systemic monocytes/macrophages that always migrate from the spleen [41] and the bone marrow [42, 43]. The appropriate infiltrated macrophages can facilitate the clearance of necrotic debris and tissue repair. However, the excessive infiltrated macrophages can lead to a burst of inflammation, which contributes to the aggravation of myocardial remodeling after MI. Our study revealed that compared to that in the MI + IgG group, the administration of Anti-Neo1 significantly further decreased the number of spleen $CD11b^+$

◂**Fig. 3** Macrophage neogenin (Neo1) deficiency enhanced cardiac fibrosis and cardiomyocyte apoptosis in mice challenged with myocardial infarction (MI), **a**, **b** PSR staining was used to analyzed cardiac fibrosis areas 21 days after MI, n = 5 in each group, unpaired Student's t-test; **c**, **d** The mRNA levels of Collagen I and Collagen III after MI, n = 6 in each group, two way analysis of variance (ANOVA) followed by Tukey's test; **e**, **h** Western blot bands of Bax and Bcl-2 and the relative protein levels 3 days after MI, n = 4 in each group, two way ANOVA followed by Tukey's test; **i** Cleaved-caspase3 (c-caspase3) expression (red) was evaluated by immunofluorescence 3 days after MI, n = 4 in each group; **j**, **k** TdT-mediated dUTP nick-end-labeling (TUNEL) assay (green) in each group 3 days after MI, n = 4, two way ANOVA followed by Tukey's test; **l**, **m** PSR staining was used to analyzed cardiac fibrosis areas 21 days after MI in MI + Neo1$^{F/F}$ and MI + Neo1$^{F/F}$;Cx3cr1^{cre} groups, n = 5, unpaired Student's t-test; **n**, **o** Western blot bands of Bax and Bcl-2 and the relative protein levels 3 days after MI in Neo1$^{F/F}$ and Neo1$^{F/F}$;Cx3cr1^{cre} mice, n = 5, two way ANOVA followed by Tukey's test; **p**, **q** Double staining of TUNEL (green) and cTnI (red) was used to analyzed cardiomyocyte apoptosis 3 days after MI in MI + Neo1$^{F/F}$ and MI + Neo1$^{F/F}$;Cx3cr1^{cre} groups, n = 4, unpaired Student's t-test. Data are expressed as the mean ± SEM. In (**b**–**d**), **f**–**h** and (k) *p < 0.05 vs. Sham + IgG group, #p < 0.05 vs. MI + IgG group; in (**m**), (**0**) and (**q**), *p < 0.05 vs. Sham + Neo1$^{F/F}$ group, #p < 0.05 vs. MI + Neo1$^{F/F}$ group

and CD11b^{+}Ly6C^{high} monocytes (Fig. S6a-d), contributing to the migration of spleen monocytes/macrophages to the heart in mice challenged with MI. Then, we evaluated the effect of Anti-Neo1 on the macrophage phenotype in vivo by flow cytometry and IF analysis. The results showed that compared to the MI + IgG group, supplementation with Anti-Neo1 significantly increased the proportion of proinflammatory macrophages (CD11b^{+}F4/80^{+}Ly6C^{high}) (Fig. 4d–f). IF staining also verified this effect, as illustrated by the increases in CD86^{+} macrophages (Fig. 4g) and i-NOS expression (Fig. 4h). In summary, functionality deficiency of Neo1 could accelerate macrophage infiltration into the ischemic myocardium and promote macrophage transformation to a proinflammatory phenotype in mice challenged with acute MI.

The regulatory effect of Neo1 on macrophages was also evaluated in Neo1$^{F/F}$;Cx3cr1^{cre} mice. Flow cytometry showed that compared to those in the MI + Neo1$^{F/F}$ group, the number and proportion of CD11b^{+}F4/80^{+} macrophages were significantly increased in the hearts of mice in the MI + Neo1$^{F/F}$;Cx3cr1^{cre} group 3 days after MI (Fig. 4i–k). In the spleen, the numbers of CD45^{+}CD11b^{+}, CD45^{+}CD11b^{+}Ly6C^{high} and CD45^{+}CD11b^{+}Ly6C^{mid} monocytes were significantly lower in the MI + Neo1$^{F/F}$;Cx3cr1^{cre} group than in the MI + Neo1$^{F/F}$ group (Fig. S7a–d). For macrophage polarization, compared to that in the MI + Neo1$^{F/F}$ group, the proportion of CD11b^{+}F4/80^{+}Ly6C^{high}CD86^{+} proinflammatory macrophages in the heart was significantly increased in the MI + Neo1$^{F/F}$;Cx3cr1^{cre} group 3 days after MI (Fig. 4l–n). In addition, IF staining also showed that the CD86-positive cells were obviously increased in the MI + Neo1$^{F/F}$;Cx3cr1^{cre} group (Fig. 4o). These results suggested that macrophage-specific Neo1 deficiency promoted monocyte/macrophage transfer from the spleen to the ischemic heart and facilitated the polarization of proinflammatory macrophages after MI.

Finally, the effect of Neo1 on macrophage phenotype was also evaluated in BMDMs in vitro. In this part, LPS + IFN-γ was used to induce the proinflammatory phenotype. Flow cytometry revealed that F4/80^{+}CD86^{+} proinflammatory macrophages were more abundant in the LPS + IFN-γ group than in the vehicle group (Fig. 4p and q). The administration of Anti-Neo1 significantly enhanced this trend (Fig. 4p and q), suggesting that Neo1 deficiency could enhance macrophage transformation to the proinflammatory phenotype in vitro. In summary, these in vivo and in vitro results indicated that Neo1 deficiency could promote the infiltration of macrophages and proinflammatory polarization, which contributes to the deterioration of myocardial remodeling after MI.

Macrophage Neo1 deficiency exacerbated the inflammatory response and impaired inflammation resolution

RT–qPCR showed that proinflammatory cytokines, including TNF-α, IL-1β and IL-6, were significantly increased at the infarction border zone after MI (Fig. 5a–c). ELISA showed that serum TNF-α and IL-1β were also increased in the MI + IgG group (Fig. 5d and e). The administration of Anti-Neo1 further significantly increased the expression of these proinflammatory cytokines at the infarction border zone (Fig. 5a-c) and in serum (Fig. 5d and e). In addition, the administration of Anti-Neo1 enhanced the expression of p-ERK but not P38 or JNK (Fig. S8a-d), indicating that the ERK signaling pathway might contribute to the increase in proinflammatory cytokines. Similarly, the mRNA levels of TNF-α, IL-1β and IL-6 were evaluated at the infarction border zone 3 days after MI in mice with macrophage-specific Neo1 deficiency. RT–qPCR showed that the mRNA levels of TNF-α, IL-1β and IL-6 were significantly higher in the MI + Neo1$^{F/F}$;Cx3cr1^{cre} group than in the MI + Neo1$^{F/F}$ group (Fig. 5f–h). These results indicated that macrophage Neo1 deficiency exacerbated the inflammatory response after MI.

Inflammation resolution has emerged as a critical endogenous process that protects the host from excessive MI-induced inflammation, contributing to improvements in myocardial remodeling and cardiac function [3]. Inflammation resolution can be illustrated by an increase in apoptotic neutrophils and an increase in macrophage

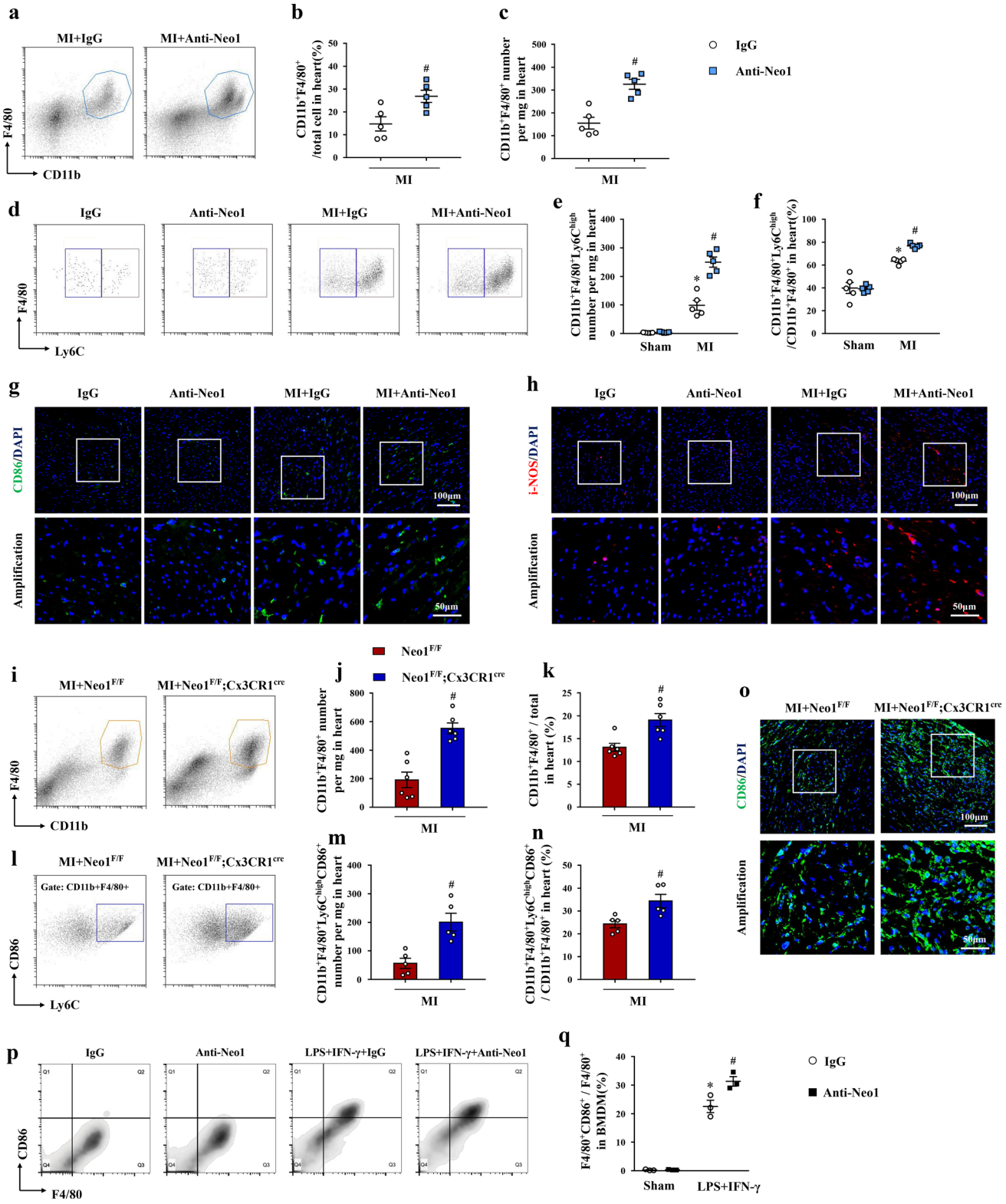
a
MI+IgG
MI+Anti-Neo1
F4/80
CD11b
b
CD11b+F4/80+ /total cell in heart(%)
MI
c
CD11b+F4/80+ number per mg in heart
IgG
Anti-Neo1
d
IgG
Anti-Neo1
MI+IgG
MI+Anti-Neo1
F4/80
Ly6C
e
CD11b+F4/80+Ly6Chigh number per mg in heart
Sham
MI
f
CD11b+F4/80+Ly6Chigh /CD11b+F4/80+ in heart(%)
g
CD86/DAPI
Amplification
100μm
50μm
h
i-NOS/DAPI
i
MI+Neo1F/F
MI+Neo1F/F;Cx3CR1cre
j
Neo1F/F
Neo1F/F;Cx3CR1cre
CD11b+F4/80+ number per mg in heart
k
CD11b+F4/80+ / total in heart (%)
l
Gate: CD11b+F4/80+
CD86
Ly6C
m
CD11b+F4/80+Ly6ChighCD86+ number per mg in heart
n
CD11b+F4/80+Ly6ChighCD86+ / CD11b+F4/80+ in heart (%)
o
p
LPS+IFN-γ+IgG
LPS+IFN-γ+Anti-Neo1
q
F4/80+CD86+ / F4/80+ in BMDM(%)
LPS+IFN-γ

◂**Fig. 4** Macrophage neogenin (Neo1) deficiency promoted macrophage infiltration and transformation to a proinflammatory phenotype, **a–c** $CD11b^+F4/80^+$ macrophages in ischemic heart were analyzed by Flow cytometry 3 days after MI, and $CD11b^+F4/80^+$ macrophages / total cell ratio and $CD11b^+F4/80^+$ macrophages number were calculated, n = 5 in each group, unpaired Student's t-test; **d–f** Proinflammatory macrophages ($CD11b^+F4/80^+Ly6C^{high}$) were analyzed by Flow cytometry 3 days after MI and the number and proportion of proinflammatory macrophages were also calculated, n = 5 in each group, two way analysis of variance (ANOVA) followed by Tukey's test; **g** CD86 positive macrophages (green) were evaluated by immunofluorescence 3 days after MI, n = 4 in each group; **h** Inducible nitric oxide synthase (i-NOS) (red) expression was evaluated by immunofluorescence 3 days after MI, n = 4 in each group; **i–k** $CD11b^+F4/80^+$ macrophages in ischemic heart were analyzed by Flow cytometry 3 days after MI in MI + $Neo1^{F/F}$ and MI + $Neo1^{F/F}$;$Cx3cr1^{cre}$ groups, and $CD11b^+F4/80^+$ macrophages / total cell ratio and $CD11b^+F4/80^+$ macrophages number were calculated, n = 5, unpaired Student's t-test; **l–n** Proinflammatory macrophages ($CD11b^+F4/80^+Ly6C^{high}CD86^+$) were analyzed by Flow cytometry 3 days after MI in MI + $Neo1^{F/F}$ and MI + $Neo1^{F/F}$;$Cx3cr1^{cre}$ groups, and the number and proportion of proinflammatory macrophages were also calculated, n = 5, unpaired Student's t-test; **o** CD86 positive macrophages (green) were evaluated by immunofluorescence 3 days after MI in MI + $Neo1^{F/F}$ and MI + $Neo1^{F/F}$;$Cx3cr1^{cre}$ groups, n = 4; **p**, **q** In bone marrow derived-macrophages (BMDMs), and the $F4/80^+CD86^+$ proinflammatory phenotype was evaluated by flow cytometry in each group 12 h after LPS + IFN-γ stimulation, and an Anti-Neo1 was administered 0.5 h before LPS + IFN-γ stimulation, n = 3, two way ANOVA followed by Tukey's test. Data are expressed as the mean ± SEM. In (**b–c**) and (**e–f**), *p < 0.05 vs. Sham + IgG group, #p < 0.05 vs. MI + IgG group; In (**j–k**) and (**m–n**), #p < 0.05 vs. MI + $Neo1^{F/F}$ group; in (**q**), *p < 0.05 vs. Sham + IgG group, # p < 0.05 vs. LPS + IFN-γ + IgG group

efferocytosis/phagocytosis. A higher proportion of neutrophils phagocytized by macrophages will facilitate the resolution of acute inflammation. In this study, we found that both administration of Anti-Neo1 and macrophage-specific Neo1 deficiency could reduce the proportion of $CD11b^+F4/80^+Ly6C^{low}MerTk^+$ macrophages (Fig. 5i–l), which can phagocytize apoptotic cells, such as apoptotic neutrophils and cardiomyocytes, in the ischemic myocardium. The ratio of neutrophils associated with macrophages ($CD11b^+Ly6G^+F4/80^+$) to total neutrophils ($CD11b^+Ly6G^+$) was significantly decreased by macrophage-specific Neo1 deficiency (Fig. 5m and n). These results suggested that Neo1 deficiency could impair macrophage phagocytosis and impede the inflammation resolution process. In addition, compared to that in the MI + IgG group, the number of apoptotic neutrophils was decreased by Anti-Neo1 (Fig. 5o), further emphasizing that the resolution of these infiltrated neutrophils was impaired.

Absolute quantitative lipidomics found that Anti-Neo1 had a regulatory effect on lipid metabolism, in which PS(18:0/20:4)-H (Fig. S9a) was significantly decreased and LPC(18:0) + HCOO (Fig. S9a) were significantly increased (Fig. 5p and q). PS (phosphatidylserine) is expressed on apoptotic cells and is an important "eat-me" signal. In efferocytosis, PS mediates the recognition and subsequent phagocytosis of macrophages on apoptotic cells [44]. Lysophosphatidylcholine (LPC), which is the main component of oxidatively damaged low-density lipoprotein, can induce the migration of macrophages, increase the production of proinflammatory cytokines and promote the progression of inflammatory diseases [45]. Therefore, the decrease in PS and the increase in LPC induced by Anti-Neo1 (Fig. 5p and q) also suggested that Neo1 deficiency impaired the clearance of apoptotic cells and the resolution of inflammation after MI.

Chemerin receptor 23 (ChemR23), formyl-peptide receptor-2 (FPR2) and G protein-coupled receptor 37 (GPR37), which are all G protein-coupled receptors, are specialized pro-resolving lipid mediators and can promote inflammation resolution in MI or ischemic stroke [46–48]. In our study, we found that the expression levels of ChemR23, FPR2 and GPR37 were inhibited by the administration of Anti-Neo1 (Fig. S10a–f), which might impair inflammation resolution mediated by these receptors. Based on these results, we concluded that Neo1 deficiency effectively impaired macrophage-mediated inflammation resolution and aggravated the inflammatory response after MI.

Neo1 deficiency promoted macrophage polarization to the proinflammatory phenotype through the JAK1-STAT1 signaling pathway

Previous studies suggested that the STAT1, STAT6 and P65 signaling pathways play key roles in the regulation of macrophage polarization and function [49]. To clarify the mechanisms by which Neo1 regulates macrophage polarization, the expression of p-STAT1, p-STAT6 and p-P65 in vivo was analyzed by western blotting and IF analysis. The results revealed that Anti-Neo1 could significantly increase the expression of p-STAT1 but not p-STAT6 or p-P65 3 days after MI (Fig. 6a, d–f). IF double staining showed that the expression of p-STAT1 in macrophages was higher in the MI + Anti-Neo1 group than in the MI + IgG group (Fig. 6g). However, there was no significant difference in p-STAT6 and p-P65 between the MI + IgG and MI + Anti-Neo1 groups (Fig. S11a and b). JAK1 and JAK2 are upstream molecules of STAT1 and were subsequently evaluated by western blotting. The results showed that Anti-Neo1 could significantly increase the expression of p-JAK1 but not p-JAK2 (Fig. 6a–c), indicating that Neo1 inhibition regulated macrophage phenotype and function possibly through the JAK1-STAT1 signaling pathway. In addition, JAK1-STAT1 pathway was also evaluated in mice with macrophage-specific Neo1 deficiency. Western blotting showed that compared to the MI + $Neo1^{F/F}$ group, the expression levels of p-JAK1 and p-STAT1 were also significantly increased in

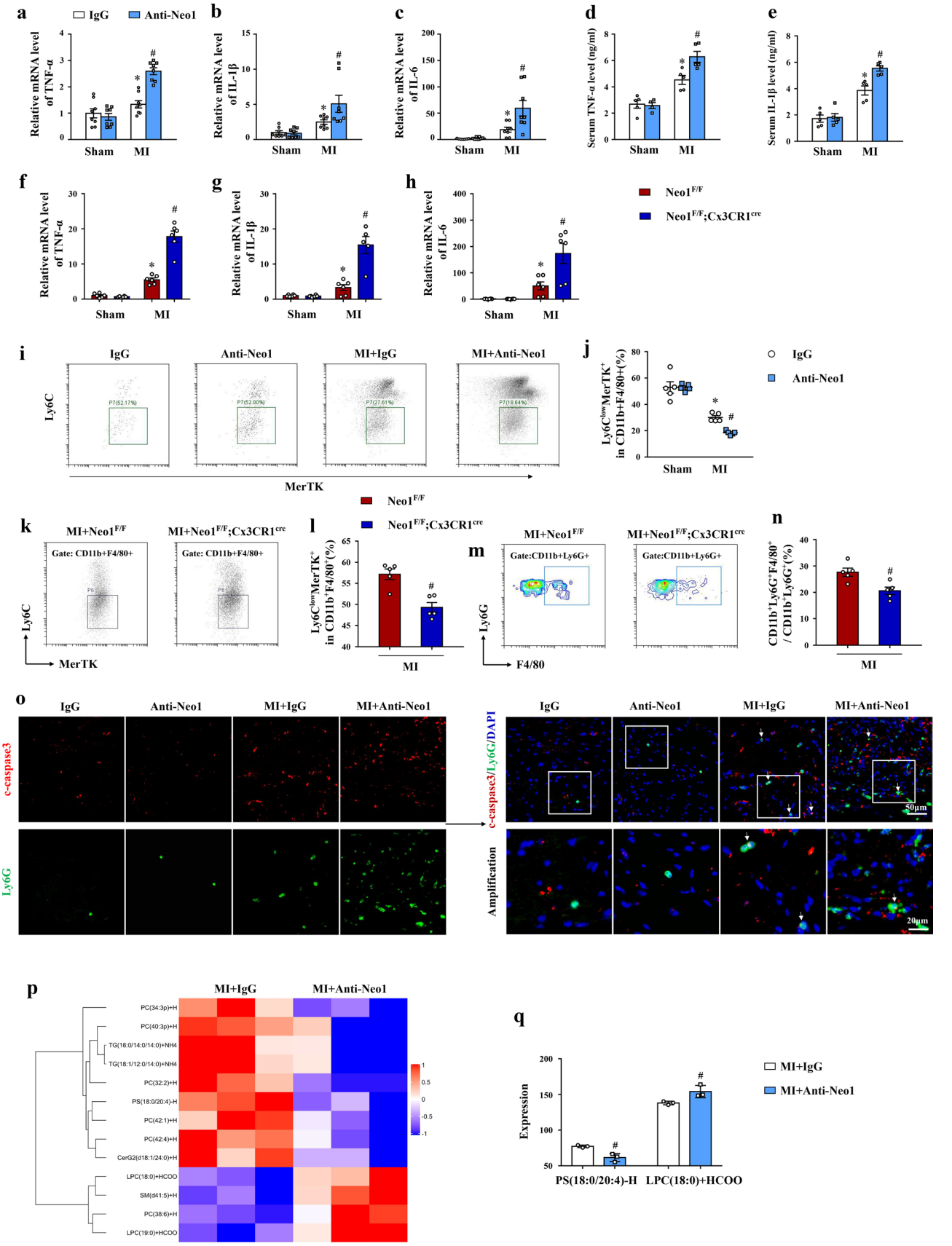
a
IgG
Anti-Neo1
Relative mRNA level of TNF-α
Sham
MI
b
Relative mRNA level of IL-1β
c
Relative mRNA level of IL-6
d
Serum TNF-α level (ng/ml)
e
Serum IL-1β level (ng/ml)
f
g
h
Neo1F/F
Neo1F/F;Cx3CR1cre
i
IgG
Anti-Neo1
MI+IgG
MI+Anti-Neo1
Ly6C
MerTK
P7(52.17%)
P7(52.00%)
P7(27.61%)
P7(16.64%)
j
Ly6Clow MerTK+ in CD11b+F4/80+(%)
k
MI+Neo1F/F
MI+Neo1F/F;Cx3CR1cre
Gate: CD11b+F4/80+
P6
l
Ly6Clow MerTK+ in CD11b+F4/80+(%)
m
Gate:CD11b+Ly6G+
Ly6G
F4/80
n
CD11b+Ly6G+F4/80+ / CD11b+Ly6G+(%)
o
c-caspase3
Ly6G
c-caspase3/Ly6G/DAPI
Amplification
50μm
20μm
p
PC(34:3p)+H
PC(40:3p)+H
TG(16:0/14:0/14:0)+NH4
TG(18:1/12:0/14:0)+NH4
PC(32:2)+H
PS(18:0/20:4)-H
PC(42:1)+H
PC(42:4)+H
CerG2(d18:1/24:0)+H
LPC(18:0)+HCOO
SM(d41:5)+H
PC(38:6)+H
LPC(19:0)+HCOO
q
Expression
PS(18:0/20:4)-H
LPC(18:0)+HCOO
MI+IgG
MI+Anti-Neo1

◂**Fig. 5** Macrophage neogenin (Neo1) deficiency exacerbated the inflammatory response and impaired the resolution of inflammation, **a**–**c** The mRNA levels of tumor necrosis factor α (TNF-α), interleukin (IL)-1β and IL-6 3 days after myocardial infarction (MI), n = 6 in each group, two way analysis of variance (ANOVA) followed by Tukey's test; **d**, **e** Serum levels of TNF-α and IL-1β were evaluated 3 days after MI, n = 5 in each group, two way ANOVA followed by Tukey's test; **f**, **h** The mRNA levels of TNF-α, IL-1β and IL-6 3 days after MI in MI + Neo1$^{F/F}$ and MI + Neo1$^{F/F}$;Cx3cr1^{cre} groups, n = 5–6, two way ANOVA followed by Tukey's test; **i**, **j** The proportion of CD11b^{+}F4/80^{+}Ly6C^{low}MerTk^{+} macrophages that have an obvious ability to phagocytize apoptotic neutrophils in the ischemic myocardium and contribute to the resolution of inflammation, was evaluated in each group 3 days after MI, n = 5, two way ANOVA followed by Tukey's test; **k**, **l** The proportion of CD11b^{+}F4/80^{+}Ly6C^{low}MerTk^{+} macrophages was also analyzed by flow cytometry in MI + Neo1$^{F/F}$ and MI + Neo1$^{F/F}$;Cx3cr1^{cre} groups, n = 5, unpaired Student's t-test; **m**, **n** The ratio of neutrophils associated with macrophages (CD11b^{+}Ly6G^{+}F4/80^{+}) to total neutrophils (CD11b^{+}Ly6G^{+}) were analyzed by flow cytometry, n = 5 in each group, unpaired Student's t-test; **o** The double-labelling immunofluorescence of cleaved-caspase3 (c-caspase3) (red) and Ly6G (neutrophil) (green) was analyzed 3 days after MI, n = 4 in each group; **p** Absolute quantitative lipidomics were performed in MI + IgG and MI + Anti-Neo1 groups and heat map showed the differential lipid molecules ($p < 0.05$), n = 3 in each group; **q** PS(18:0/20:4)-H and LPC(18:0) + HCOO were shown in each group, n = 3, # indicating $p < 0.05$ and variable importance for the projection (VIP) > 1 vs. MI + IgG group. Data are expressed as the mean ± SEM. In (**a**–**e**) and (**j**) *$p < 0.05$ vs. Sham + IgG group, #$p < 0.05$ vs. MI + IgG group; in (**f**–**h**), (**l**) and (**n**) *$p < 0.05$ vs. Sham + Neo1$^{F/F}$ group, #$p < 0.05$ vs. MI + Neo1$^{F/F}$ group

MI + Neo1$^{F/F}$;Cx3cr1^{cre} group (Fig. 6h–j), which further emphasized that Neo1 may regulate macrophage polarization through JAK-STAT1 signaling pathway.

The mechanisms by which Neo1 affects macrophage polarization were also explored in vitro. In BMDMs, we demonstrated that the administration of LPS + IFN-γ increased the expression of p-JAK1 and p-STAT1 (Fig. 6k), which was further increased by treatment with Anti-Neo1 (Fig. 6k). Confocal microscopy showed that Anti-Neo1 not only increased p-STAT1 expression but also promoted p-STAT1 entry into the nucleus (Fig. 6l), resulting in the proinflammatory polarization. Therefore, Neo1 deficiency could promote macrophage transformation to the proinflammatory phenotype via the JAK1-STAT1 signaling pathway.

Blockade of the STAT1 signaling pathway abolished the effect of Neo1 on macrophage polarization, the inflammatory response and inflammation resolution

Flu was used to inhibit STAT1 activation. In our study, we demonstrated that Flu significantly decreased the expression of p-STAT1 (Fig. 7a). Compared to that in the MI + Anti-Neo1 group, Flu significantly inhibited the increased infiltration of CD11b^{+}F4/80^{+} macrophages (Fig. 7b) in left ventricular tissue 3 days after MI. In addition, Anti-Neo1 promoted macrophage transformation to the proinflammatory phenotype (CD11b^{+}F4/80^{+}Ly6C^{high}), which was blocked by the administration of Flu in vivo (Fig. 7c). Similarly, in LPS + IFN-γ-treated BMDMs, the administration of Flu abolished the effect of Anti-Neo1 on proinflammatory polarization (F4/80^{+}CD86^{+}) (Fig. 7d).

Next, the effect of Flu on the inflammatory response was evaluated by RT–qPCR. The results showed that supplementation with Flu abrogated the Anti-Neo1-induced increase in the expression of TNF-α, IL-1β and IL-6 in the infarcted border zone of cardiac tissue in mice 3 days after MI (Fig. 7e). During inflammation resolution, we found that compared to MI + Anti-Neo1 treatment, Flu treatment increased the proportion of CD11b^{+}F4/80^{+}Ly6C^{low}MerTk^{+} macrophages (Fig. 7f), indicating that Flu could restore macrophage efferocytosis and promote inflammation resolution.

Blocking the STAT1 signaling pathway abolished the effect of Neo1 on cardiomyocyte apoptosis, cardiac function, cardiac fibrosis and infarction size

First, cardiomyocyte apoptosis was evaluated. The results showed that Flu could abolish the increase in cardiomyocyte apoptosis induced by treatment with Anti-Neo1 3 days after MI in mice, as illustrated by the decreased expression of Bax and c-caspase3 (Fig. 8a). Then, cardiac function was analyzed by echocardiography before MI and at 3 d, 7 d, and 21 d after MI. Neo1 inhibition exacerbated cardiac dysfunction at 3 d, 7 d and 21 d. However, Flu treatment blocked the Anti-Neo1-induced exacerbation of cardiac dysfunction at the indicated time points, as illustrated by the decreases in LVEDd and LVEDs (Fig. S12b and c) and the increases in LVEF and LVFS (Fig. 8b-d). There were no significant differences in heart rate among groups at different time points (Fig. S12a). In addition, to further evaluate myocardial remodeling after MI, infarction size and cardiac fibrosis were analyzed. Compared to that in the MI + Anti-Neo1 group, Flu treatment reduced infarction size 21 days after MI (Fig. 8e). Similarly, Flu treatment reduced the cardiac fibrosis area (Fig. 8f), as illustrated by PSR staining 21 days after MI. These results suggested that Flu could abolish Neo1 deficiency-induced exacerbation of myocardial remodeling in mice challenged with MI.

Neo1 overexpression inhibited macrophage transformation to a proinflammatory phenotype

To induce Neo1 overexpression, a Neo1-overexpressing adenovirus (ad-Neo1) was transfected into BMDMs, as evidenced by EGEP staining (Fig. S13a). Compared to the adenovirus-negative control (ad-NC), ad-Neo1 dramatically increased the expression of Neo1 (Fig. S13b). Neo1

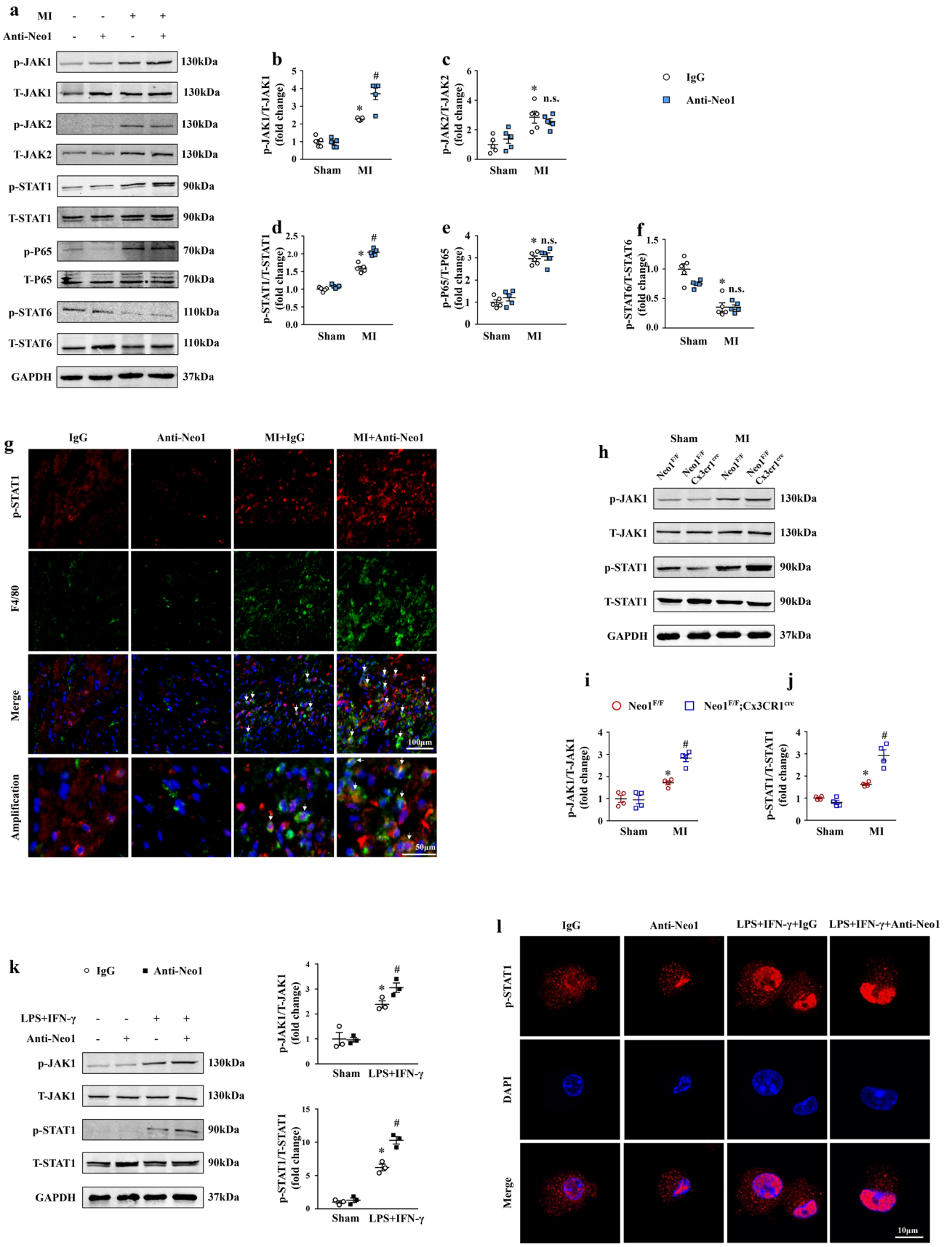
a
MI
Anti-Neo1
p-JAK1
T-JAK1
p-JAK2
T-JAK2
p-STAT1
T-STAT1
p-P65
T-P65
p-STAT6
T-STAT6
GAPDH
130kDa
90kDa
70kDa
110kDa
37kDa
b
p-JAK1/T-JAK1 (fold change)
c
p-JAK2/T-JAK2 (fold change)
IgG
Anti-Neo1
d
p-STAT1/T-STAT1 (fold change)
e
p-P65/T-P65 (fold change)
f
p-STAT6/T-STAT6 (fold change)
Sham
MI
n.s.
g
IgG
Anti-Neo1
MI+IgG
MI+Anti-Neo1
p-STAT1
F4/80
Merge
Amplification
100μm
50μm
h
Sham
MI
Neo1F/F
Neo1F/F Cx3cr1cre
i
Neo1F/F
j
Neo1F/F;Cx3CR1cre
k
LPS+IFN-γ
Anti-Neo1
l
LPS+IFN-γ+IgG
LPS+IFN-γ+Anti-Neo1
DAPI
10μm

◂**Fig. 6** Neogenin (Neo1) deficiency promoted macrophage transformation to the proinflammatory phenotype through the janus kinase 1 (JAK1)-signal transduction and activator of transcription 1 (STAT1) signal pathway, not STAT6 and P65 pathways, **a** The protein bands of p/T-JAK1, p/T-JAK2, p/T-STAT1, p/T-P65, p/T-STAT6 and GAPDH 3 days after myocardial infarction (MI), n = 5 in each group; **b-f** Quantitative analysis of p-JAK1, p-JAK2, p-STAT1, p-P65 and p-STAT6 in each group 3 days after MI, n = 5, two way ANOVA followed by Tukey's test; **g** The double-labelling immunofluorescence of p-STAT1 and F4/80 3 days after MI, n = 4 in each group; **h** The protein bands of p/T-JAK1 and p/T-STAT1 3 days after MI in $Neo1^{F/F}$ and $Neo1^{F/F}$;$Cx3cr1^{cre}$ mice; **i**, **j** Quantitative analysis of p-JAK1 and p-STAT1 in each group 3 days after MI in $Neo1^{F/F}$ and $Neo1^{F/F}$;$Cx3cr1^{cre}$ mice, n = 5, two way ANOVA followed by Tukey's test; **k** The protein bands and quantitative analysis of p/T-JAK1 and p/T-STAT1 in bone marrow derived-macrophages (BMDMs) 12 h after stimulation with LPS + IFN-γ, n = 3 in each group, two way ANOVA followed by Tukey's test; **l** The immunofluorescence of p-STAT1 in BMDMs was analyzed by a confocal laser scanning microscope, n = 3 in each group. Data are expressed as the mean ± SEM. In **b-f**, *p < 0.05 vs. Sham + IgG group, #p < 0.05 vs. MI + IgG group, n.s. indicating no significance; in **i** and **j** *p < 0.05 vs. Sham + $Neo1^{F/F}$ group, #p < 0.05 vs. MI + $Neo1^{F/F}$ group; in **k**, *p < 0.05 vs. Sham + IgG group, #p < 0.05 vs. LPS + IFN-γ + IgG group

overexpression inhibited macrophage transformation to a proinflammatory phenotype in vitro, as illustrated by the decreased proportion of $F4/80^{+}CD86^{+}$ macrophages (Fig. S13c). Western blotting revealed that Neo1 overexpression inhibited the expression of p-STAT1 (Fig. S13d). Confocal microscopy showed that Neo1 overexpression inhibited both the expression of p-STAT1 and the translocation of p-STAT1 from the cytoplasm to the nucleus (Fig. S13e). Therefore, Neo1 overexpression could inhibit macrophage transformation to a proinflammatory phenotype through the JAK1-STAT1 signaling pathway.

Discussion

In our study, we first revealed that the expression of Neo1 was decreased during the early stage and was subsequently increased in the late stage at the infarction border zone in MI mice. Macrophage-specific Neo1 deficiency exacerbated inflammation and myocardial remodeling after MI, as illustrated by the exacerbation of the inflammatory response, dysregulation of inflammation resolution, increase in infarction size and aggravation of cardiac dysfunction, cardiomyocyte apoptosis and cardiac fibrosis. The mechanisms may be associated with macrophage transformation to the proinflammatory phenotype, which is regulated by the JAK1-STAT1 signaling pathway.

Neo1, a multifunctional transmembrane receptor, belongs to the Ig superfamily. Neo1 has been shown to play a role in neural development by binding the axon guidance cue netrin-1 and RGMs [14–16]. In addition to its traditional function, Neo1 also plays a critical role in the immune response and inflammation [12]. A previous study revealed that Neo1 inhibition could promote the resolution of inflammation in murine peritonitis, as evidenced by the suppression of neutrophil migration, increase in neutrophil apoptosis and increased endogenous biosynthesis of specialized proresolving mediators [20]. In rodents with MI, netrin-1 promoted the survival and migration of mesenchymal stem cells, protecting against MI-induced ischemic injuries [50]. Similarly, the protective effect of netrin-1 against ischemia–reperfusion injury has also been reported in several studies, and the mechanisms might be associated with myeloid adenosine A2b signaling [51], nitric oxide production [52] and the preservation of mitochondrial integrity [53]. Therefore, Neo1 may play a key role in MI by regulating inflammation. Since Neo1 is a critical molecule of the axon guidance pathway, we first conducted enrichment and analysis of the axon guidance pathway in the left ventricular tissue of mice after MI. The results showed that Neo1 expression was significantly decreased in the MI group. Then, to clarify the association between Neo1 and MI, the expression levels of Neo1 were further evaluated at the infarction border zone of mice with MI. Our study revealed that the expression levels of Neo1 were significantly decreased in the early stage and were subsequently increased in the late stage after MI. Furthermore, we found that Neo1 was expressed in macrophages in vivo and in vitro, and its expression was decreased in proinflammatory macrophages. Then, a Neo1 neutralizing antibody and $Neo1^{F/F}$;$Cx3cr1^{cre}$ mice were separately used to implement Neo1 deficiency. Our study showed that Neo1 deficiency exacerbated myocardial remodeling after MI in mice, as evidenced by the increase in infarction size, increase in cardiac fibrosis, exacerbation of cardiomyocyte apoptosis and worsening of cardiac dysfunction.

Inflammation is an important mechanism of myocardial remodeling after MI. The extensive infiltration of immune cells and excessive secretion of inflammatory cytokines exacerbate cardiomyocyte apoptosis and adverse left ventricular remodeling after MI [54]. However, the attenuation of inflammation through different methods, such as CD226 deletion [55], IL-35 treatment [34] and inhibition of glucose

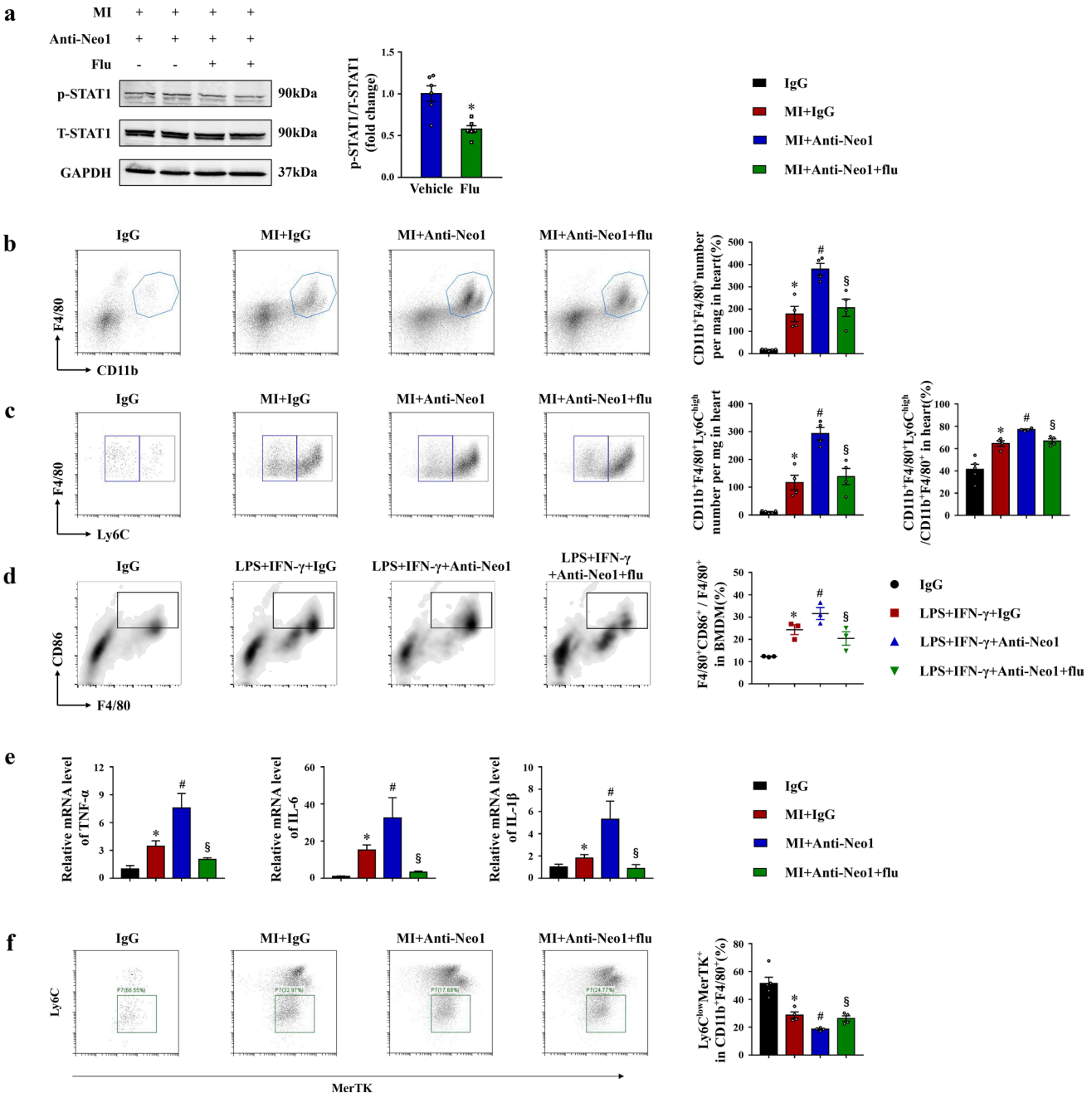

Fig. 7 Blockade of STAT1 signaling pathway reversed the effect of neogenin (Neo1) on macrophage polarization, inflammatory response and inflammation resolution, **a** Fludarabine phosphate (Flu) was used to block the activation of signal transduction and activator of transcription 1 (STAT1) and was administered on day 1 before myocardial infarction (MI) and every other day from day 1 to day 21 after MI, and the protein level of p-STAT1 was evaluated after the administration of Flu, n = 6 in each group, unpaired Student's t-test; **b** The infiltration of $CD11b^+F4/80^+$ macrophages in the ischemic myocardium was analyzed by flow cytometry 3 days after MI, n = 4–5 in each group, one way analysis of variance (ANOVA) followed by Tukey's test; **c** Proinflammatory macrophages ($CD11b^+F4/80^+Ly6C^{high}$) in the ischemic myocardium were evaluated 3 days after MI, n = 4–5 in each group, one way ANOVA followed by Tukey's test; **d** The proportion of $F4/80^+CD86^+$ macrophages in bone marrow derived-macrophages (BMDMs) was evaluated 12 h after LPS + IFN-γ stimulation, the Flu and the Neo1 neutrolizing Antibody (Anti-Neo1) were administered at 1 h and 0.5 h before LPS + IFN-γ stimulation, n = 3 in each group, one way ANOVA followed by Tukey's test; **e** The mRNA levels of tumor necrosis factor α (TNF-α), interleukin (IL)-1β and IL-6 3 days after MI, n = 8 in each group, one way ANOVA followed by Tukey's test; **f** The proportion of $CD11b^+F4/80^+Ly6C^{low}MerTk^+$ macrophages in the ischemic myocardium was evaluated in each group 3 days after MI, n = 4–5, one way ANOVA followed by Tukey's test. Data are expressed as the mean ± SEM. In (**a**), *p < 0.05 vs. Vehicle group; in (**b**–**d**) and (**f**), *p < 0.05 vs. IgG group, #p < 0.05 vs. MI + IgG group, §p < 0.05 vs. MI + Anti-Neo1 group; in (**d**), *p < 0.05 vs. IgG group, #p < 0.05 vs. LPS + IFN-γ + IgG group, §p < 0.05 vs. LPS + IFN-γ + Anti-Neo1 group

transporter 1 [56], could ultimately mitigate adverse left ventricular remodeling after MI. Macrophages, which are the predominant innate immune cells, can rapidly infiltrate the ischemic myocardium and transform into the proinflammatory phenotype in the early stage of MI, contributing to the excessive secretion of inflammatory cytokines [8, 57]. The decrease in proinflammatory macrophage polarization mediated by Dectin-1 deficiency could exert a protective effect and improve cardiac remodeling in mice with MI [11], suggesting that targeting macrophage polarization is a promising strategy to treat MI. In our study, Neo1 deficiency not only increased macrophage infiltration but also promoted proinflammatory macrophage polarization in vivo and in vitro. As a result, the inflammatory response in the heart was significantly enhanced, and pathological left ventricular remodeling was further exacerbated. In contrast, Neo1 overexpression inhibited proinflammatory polarization in vitro, which might attenuate inflammation and improve myocardial remodeling after MI.

Following MI, the natural resolution of inflammation is needed to avoid excessive inflammation. Natural resolution is initiated when neutrophils undergo apoptosis and are subsequently digested by macrophage efferocytosis/phagocytosis [58]. Promoting neutrophil apoptosis could shorten the duration of inflammation, accelerating the restoration of immune balance [59]. During the clearance of apoptotic cells, PS that is expressed on apoptotic cells and is an important "eat-me" signal mediates the recognition of apoptotic cells by macrophages and promotes macrophage efferocytosis. In addition, neutrophil apoptosis could trigger macrophage efferocytosis and promote macrophage transformation from a proinflammatory to an anti-inflammatory/reparative phenotype [59, 60], leading to improvements in left ventricular remodeling after MI. Anti-inflammatory macrophages are also accompanied by an increase in efferocytosis [61]. Several previous studies [62–64] have highlighted the crucial importance of $MerTk^{+}$ macrophages in postischemic cardiac remodeling. MerTk deficiency in macrophages could damage efferocytosis, block inflammation resolution and exacerbate cardiac remodeling. However, these changes were significantly reversed in MerTk(CR) mice that were resistant to the cleavage of membrane MerTk. Consistent with previous studies, we found that Neo1 deficiency delayed neutrophil apoptosis (evidenced by the decrease in Ly6G neutrophils that expressed c-caspase3), impaired the recognition of apoptotic cells (evidenced by the decrease in PS) and impeded macrophage efferocytosis (evidenced by the decreased ratio of neutrophils associated with macrophages:total neutrophils and the decrease in MerTK + macrophage number). In addition, ChemR23, FPR2 and GPR37 are the receptors of specialized pro-resolving lipid mediators and have positive effects on the resolution of inflammation in MI or ischemic stroke models [46–48]. In our study, Neo1 inhibition decreased the expression levels of these resolution receptors. In summary, Neo1 deficiency delayed neutrophil apoptosis, impaired macrophage efferocytosis and ultimately blocked inflammation resolution, resulting in the deterioration of pathological left ventricular remodeling after MI.

Previous studies suggested that the STAT1, P65 and STAT6 signal pathways have critical regulatory effects on macrophage polarization and phagocytosis [49, 65–67]. IFNγ can activate the JAK1/2-STAT1 pathway to induce the activation of macrophages, resulting in the transformation of macrophages to a proinflammatory phenotype [66]. Treatment with a JAK1/2 inhibitor can inhibit STAT1 pathway and activate STAT6 pathway in macrophages in vitro, contributing to a switch from a proinflammatory to an anti-inflammatory phenotype [68]. In addition, JAK1/2-STAT6 pathway mediates the promoted effects of the 78 kilodalton glucose regulated protein on M2 macrophages [69]. The activation of STAT6 is essential for the secretion of arginase1 and the maintaining of macropahge/microglia efferocytosis, contributing to the attenuation of inflammation in stroke [67]. Therefore, in our study, to determine the molecular mechanisms by which Neo1 regulates macrophage function, the protein levels of these signaling pathways were evaluated. We found that the STAT1 and P65 signaling pathways were activated and that the STAT6 signaling pathway was inhibited in MI. Neo1 deficiency enhanced the activation of JAK1-STAT1 but did not affect the JAK2, P65 and STAT6 signaling pathways. Then, Flu, a specific inhibitor of STAT1 activation, was used to clarify whether inhibition of the JAK1-STAT1 pathway could abolish the regulatory effect of Anti-Neo1 on macrophage polarization, inflammation resolution, myocardial remodeling and cardiac function in mice with MI. Our results revealed that compared to that in the MI + Anti-Neo1 group, inhibition of the JAK1-STAT1

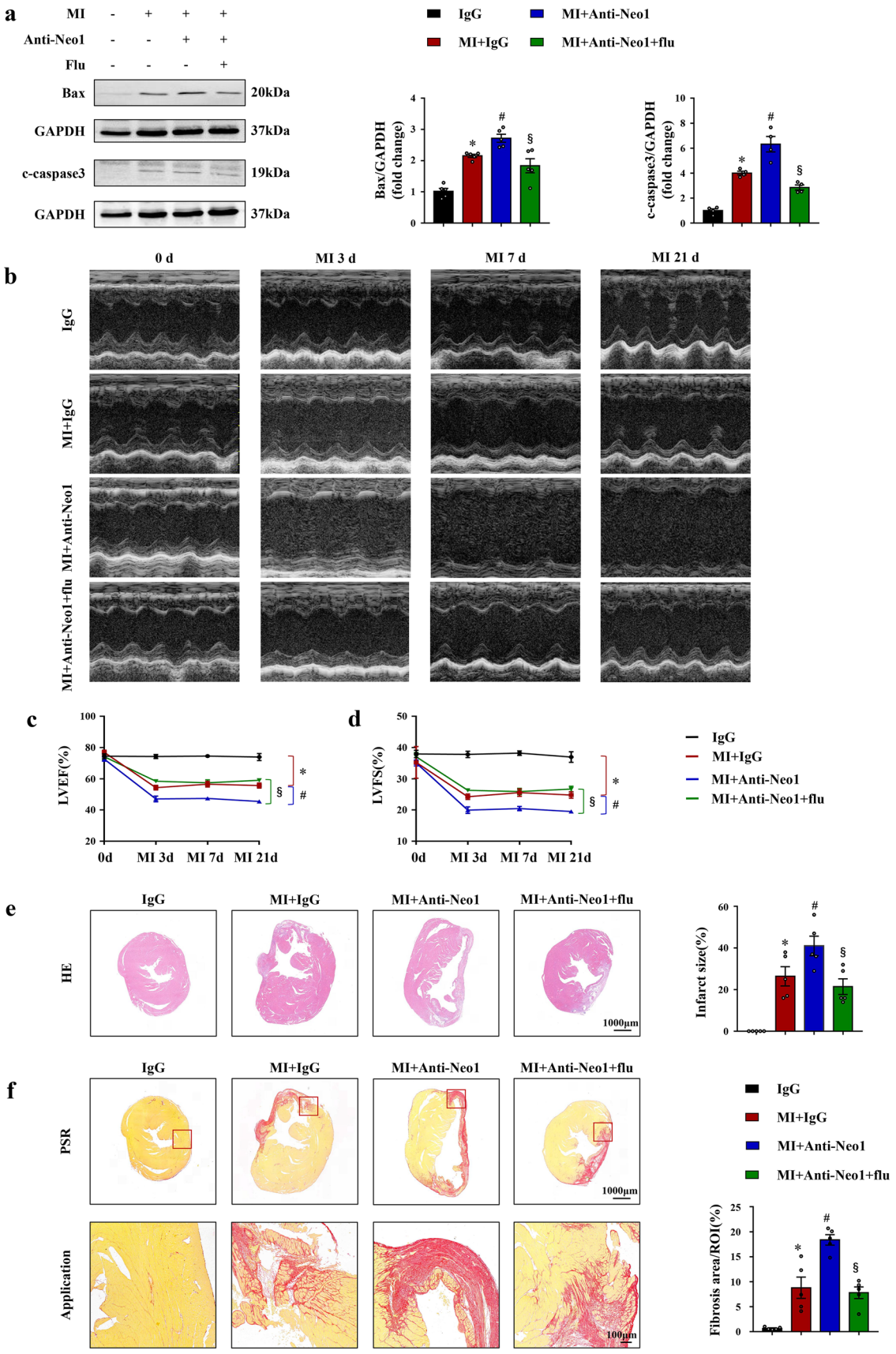
a
MI
Anti-Neo1
Flu
Bax
GAPDH
c-caspase3
GAPDH
20kDa
37kDa
19kDa
37kDa
IgG
MI+IgG
MI+Anti-Neo1
MI+Anti-Neo1+flu
Bax/GAPDH (fold change)
c-caspase3/GAPDH (fold change)
b
0 d
MI 3 d
MI 7 d
MI 21 d
IgG
MI+IgG
MI+Anti-Neo1
MI+Anti-Neo1+flu
c
LVEF(%)
0d
MI 3d
MI 7d
MI 21d
d
LVFS(%)
e
HE
Infarct size(%)
1000μm
f
PSR
Application
Fibrosis area/ROI(%)
100μm

◂**Fig. 8** Blockade of STAT1 signal pathway reversed the effect of neogenin (Neo1) on cardiomyocyte apoptosis, cardiac function, cardiac fibrosis and infarction siz, **a** The western blot bands and relative quantitative protein levels of Bax and cleaved-caspase3 (c-caspase3) 3 days after myocardial infarction (MI), n = 4–5 in each group, one way analysis of variance (ANOVA) followed by Tukey's test; **b–d** The left ventricular (LV) function, including LV ejection fraction (LVEF) and LV fraction shortening (LVFS), was performed with echocardiography before surgery and at different time points after surgery, n = 8 in each group, one way ANOVA followed by Tukey's test; **e** The representative hematoxylin–eosin (HE) staining and infarction size in each group 21 days after MI, n = 5, one way ANOVA followed by Tukey's test; **f** The representative picrosirius red (PSR) staining and cardiac fibrosis area 21 days after MI, n = 5 in each group, one way ANOVA followed by Tukey's test. Data are expressed as the mean ± SEM. *p < 0.05 vs. Sham + IgG group, # p < 0.05 vs. MI + IgG group, § p < 0.05 vs. MI + Anti-Neo1 group

pathway decreased the infiltration of macrophages, reduced the proportion of proinflammatory macrophages, inhibited the secretion of proinflammatory cytokines and promoted the resolution of inflammation, finally resulting in improvements in cardiomyocyte apoptosis, myocardial fibrosis and cardiac function. Therefore, Neo1 deficiency exacerbated inflammation and myocardial remodeling after MI by regulating the macrophage phenotype in a JAK1-STAT1 signaling pathway-dependent manner.

In conclusion, Neo1 deficiency aggravates inflammation and left ventricular remodeling after MI by modulating macrophage phenotype and function in a JAK1-STAT1 signaling pathway-dependent manner.

Supplementary Information The online version contains supplementary material available at https://doi.org/10.1007/s00018-023-04974-7.

Acknowledgements We acknowledge Model Animal Research Center, Renmin Hospital of Wuhan University, which offered enough support for our study. We also acknowledge Institute of Hydrobiology, Chinese Academy of Sciences, which offered enough support in flow cytometry.

Author contributions Literature search: JSZ, MLW, JW, Study design: JSZ, MLW, ZY, Figures: JSZ, MLW, CW, WD, MMZ, Data collection: JSZ, MLW, Data analysis: JSZ, MLW, Data interpretation: JSZ, JFL, YX, CW, Funding acquisition: MLW, JW, JJQ, Project administration: JSZ, MLW, ZY, WD, MMZ, WP, SWX, JPY, CW, Supervision: JW, JY, DY, Writing–original draft: JSZ, MLW, Writing–review & editing: MLW, JW, JJQ.

Funding National Natural Science Foundation of China, 82100292 (MLW), Excellent Doctoral Program of Zhongnan Hospital of Wuhan University, ZNYB2022001 (JJQ), National Natural Science Foundation of China, 82070436 (JW).

Data availability All data are available in the main text or the supplementary materials and all data that support the findings in this study are available from the corresponding author upon reasonable request.

Declarations

Conflict of interest The authors have no relevant financial or non-financial interests to disclose.

References

1. Anderson JL, Morrow DA (2017) Acute myocardial infarction. N Engl J Med 376:2053–2064
2. Thygesen K, Alpert JS, Jaffe AS, Chaitman BR, Bax JJ, Morrow DA et al (2018) Fourth universal definition of myocardial infarction (2018). J Am Coll Cardiol 72:2231–2264
3. Kologrivova I, Shtatolkina M, Suslova T, Ryabov V (2021) Cells of the Immune system in cardiac remodeling: main players in resolution of inflammation and repair after myocardial infarction. Front Immunol 12:664457
4. Nahrendorf M, Swirski FK, Aikawa E, Stangenberg L, Wurdinger T, Figueiredo JL et al (2007) The healing myocardium sequentially mobilizes two monocyte subsets with divergent and complementary functions. J Exp Med 204:3037–3047
5. Kain V, Prabhu SD, Halade GV (2014) Inflammation revisited: inflammation versus resolution of inflammation following myocardial infarction. Basic Res Cardiol 109:444
6. Huang S, Frangogiannis NG (2018) Anti-inflammatory therapies in myocardial infarction: failures, hopes and challenges. Br J Pharmacol 175:1377–1400
7. Ridker PM, Everett BM, Thuren T, MacFadyen JG, Chang WH, Ballantyne C et al (2017) Antiinflammatory therapy with Canakinumab for atherosclerotic disease. N Engl J Med 377:1119–1131
8. Liu S, Chen J, Shi J, Zhou W, Wang L, Fang W et al (2020) M1-like macrophage-derived exosomes suppress angiogenesis and exacerbate cardiac dysfunction in a myocardial infarction microenvironment. Basic Res Cardiol 115:22
9. Bejerano T, Etzion S, Elyagon S, Etzion Y, Cohen S (2018) Nanoparticle delivery of miRNA-21 mimic to cardiac macrophages improves myocardial remodeling after myocardial infarction. Nano Lett 18:5885–5891
10. Li Y, Dong M, Wang Q, Kumar S, Zhang R, Cheng W et al (2021) HIMF deletion ameliorates acute myocardial ischemic injury by promoting macrophage transformation to reparative subtype. Basic Res Cardiol 116:30
11. Fan Q, Tao R, Zhang H, Xie H, Lu L, Wang T et al (2019) Dectin-1 contributes to myocardial Ischemia/reperfusion Injury by regulating macrophage polarization and neutrophil infiltration. Circulation 139:663–678
12. Fujita Y, Yamashita T (2017) The roles of RGMa-neogenin signaling in inflammation and angiogenesis. Inflamm Regen 37:6
13. Robinson RA, Griffiths SC, van de Haar LL, Malinauskas T, van Battum EY, Zelina P et al (2021) Simultaneous binding of guidance Cues NET1 and RGM blocks extracellular NEO1 signaling. Cell 184:2103–2120
14. Sun D, Sun XD, Zhao L, Lee DH, Hu JX, Tang FL et al (2018) Neogenin, a regulator of adult hippocampal neurogenesis, prevents depressive-like behavior. Cell Death Dis 9:8
15. Sun XD, Chen WB, Sun D, Huang J, Li YQ, Pan JX et al (2018) Neogenin in amygdala for neuronal activity and information processing. J Neurosci 38:9600–9613
16. De Vries M, Cooper HM (2008) Emerging roles for neogenin and its ligands in CNS development. J Neurochem 106:1483–1492
17. Muramatsu R, Kubo T, Mori M, Nakamura Y, Fujita Y, Akutsu T et al (2011) RGMa modulates T cell responses and is involved in autoimmune encephalomyelitis. Nat Med 17:488–494
18. Mirakaj V, Brown S, Laucher S, Steinl C, Klein G, Kohler D et al (2011) Repulsive guidance molecule-A (RGM-A) inhibits leukocyte migration and mitigates inflammation. Proc Natl Acad Sci U S A 108:6555–6560
19. Schlegel M, Granja T, Kaiser S, Korner A, Henes J, Konig K et al (2014) Inhibition of neogenin dampens hepatic ischemia-reperfusion injury. Crit Care Med 42:e610–e619

20. Schlegel M, Korner A, Kaussen T, Knausberg U, Gerber C, Hansmann G et al (2018) Inhibition of neogenin fosters resolution of inflammation and tissue regeneration. J Clin Invest 128:4711–4726
21. Iwamoto S, Itokazu T, Sasaki A, Kataoka H, Tanaka S, Hirata T et al (2022) RGMa signal in macrophages induces neutrophil-related Astrocytopathy in NMO. Ann Neurol. https://doi.org/10.1002/ana.26327
22. Feng Y, Liu J, Wang M, Liu M, Shi L, Yuan W et al (2017) The E23K variant of the Kir6.2 subunit of the ATP-sensitive potassium channel increases susceptibility to ventricular arrhythmia in response to ischemia in rats. Int J Cardiol 232:192–198
23. Li L, Wang X, Chen W, Qi H, Jiang DS, Huang L et al (2015) Regulatory role of CARD3 in left ventricular remodelling and dysfunction after myocardial infarction. Basic Res Cardiol 110:56
24. Taniyama Y, Katsuragi N, Sanada F, Azuma J, Iekushi K, Koibuchi N et al (2016) Selective blockade of Periostin Exon 17 preserves cardiac performance in acute myocardial infarction. Hypertension 67:356–361
25. Ye J, Que B, Huang Y, Lin Y, Chen J, Liu L et al (2019) Interleukin-12p35 knockout promotes macrophage differentiation, aggravates vascular dysfunction, and elevates blood pressure in angiotensin II-infused mice. Cardiovasc Res 115:1102–1113
26. Zeng G, Lian C, Yang P, Zheng M, Ren H, Wang H (2019) E3-ubiquitin ligase TRIM6 aggravates myocardial ischemia/reperfusion injury via promoting STAT1-dependent cardiomyocyte apoptosis. Aging (Albany NY) 11:3536–3550
27. Wei W, Xiao X, Li J, Ding H, Pan W, Deng S et al (2019) Activation of the STAT1 pathway accelerates periodontitis in Nos3(-/-) Mice. J Dent Res 98:1027–1036
28. Feng Z, Zheng W, Tang Q, Cheng L, Li H, Ni W et al (2017) Fludarabine inhibits STAT1-mediated up-regulation of caspase-3 expression in dexamethasone-induced osteoblasts apoptosis and slows the progression of steroid-induced avascular necrosis of the femoral head in rats. Apoptosis 22:1001–1012
29. Zhang J, Wang M, Ding W, Zhao M, Ye J, Xu Y et al (2020) Resolvin E1 protects against doxorubicin-induced cardiotoxicity by inhibiting oxidative stress, autophagy and apoptosis by targeting AKT/mTOR signaling. Biochem Pharmacol 180:114188
30. Yang G, Min D, Yan J, Yang M, Lin G (2018) Protective role and mechanism of snakegourd peel against myocardial infarction in rats. Phytomedicine 42:18–24
31. van Duijvenboden K, de Bakker D, Man J, Janssen R, Gunthel M, Hill MC et al (2019) Conserved NPPB+ border zone switches From MEF2- to AP-1-driven gene program. Circulation 140:864–879
32. Zhang J, Wang M, Ye J, Liu J, Xu Y, Wang Z et al (2020) The Anti-inflammatory mediator Resolvin E1 protects mice against lipopolysaccharide-induced heart injury. Front Pharmacol 11:203
33. Wang Z, Xu Y, Wang M, Ye J, Liu J, Jiang H et al (2018) TRPA1 inhibition ameliorates pressure overload-induced cardiac hypertrophy and fibrosis in mice. EBioMedicine 36:54–62
34. Jia D, Jiang H, Weng X, Wu J, Bai P, Yang W et al (2019) Interleukin-35 promotes macrophage survival and improves wound healing after myocardial infarction in mice. Circ Res 124:1323–1336
35. Wang M, Liu M, Zhang J, Liu J, Ye J, Xu Y et al (2020) Resolvin D1 protects against sepsis-induced cardiac injury in mice. BioFactors 46:766–776
36. Subramanian A, Tamayo P, Mootha VK, Mukherjee S, Ebert BL, Gillette MA et al (2005) Gene set enrichment analysis: a knowledge-based approach for interpreting genome-wide expression profiles. Proc Natl Acad Sci U S A 102:15545–15550
37. Mootha VK, Lindgren CM, Eriksson KF, Subramanian A, Sihag S, Lehar J et al (2003) PGC-1alpha-responsive genes involved in oxidative phosphorylation are coordinately downregulated in human diabetes. Nat Genet 34:267–273
38. Nakanishi Y, Kang S, Kumanogoh A (2022) Axon guidance molecules in immunometabolic diseases. Inflamm Regen 42:5
39. Lee WS, Lee WH, Bae YC, Suk K (2019) Axon Guidance molecules guiding Neuroinflammation. Exp Neurobiol 28:311–319
40. Kang JS, Yi MJ, Zhang W, Feinleib JL, Cole F, Krauss RS (2004) Netrins and neogenin promote myotube formation. J Cell Biol 167:493–504
41. Swirski FK, Nahrendorf M, Etzrodt M, Wildgruber M, Cortez-Retamozo V, Panizzi P et al (2009) Identification of splenic reservoir monocytes and their deployment to inflammatory sites. Science 325:612–616
42. Jiao J, He S, Wang Y, Lu Y, Gu M, Li D et al (2021) Regulatory B cells improve ventricular remodeling after myocardial infarction by modulating monocyte migration. Basic Res Cardiol 116:46
43. van Furth R, Cohn ZA (1968) The origin and kinetics of mononuclear phagocytes. J Exp Med 128:415–435
44. Doran AC, Yurdagul AJ, Tabas I (2020) Efferocytosis in health and disease. Nat Rev Immunol 20:254–267
45. Liu P, Zhu W, Chen C, Yan B, Zhu L, Chen X et al (2020) The mechanisms of lysophosphatidylcholine in the development of diseases. Life Sci 247:117443
46. Koenig AL, Lavine KJ (2021) Leveraging FPR2 agonists to resolve inflammation and improve outcomes following myocardial infarction. JACC Basic Transl Sci 6:690–692
47. Liu G, Liu Q, Shen Y, Kong D, Gong Y, Tao B et al (2018) Early treatment with resolvin E1 facilitates myocardial recovery from Ischaemia in mice. Br J Pharmacol 175:1205–1216
48. McCrary MR, Jiang MQ, Giddens MM, Zhang JY, Owino S, Wei ZZ et al (2019) Protective effects of GPR37 via regulation of inflammation and multiple cell death pathways after ischemic stroke in mice. FASEB J 33:10680–10691
49. Lawrence T, Natoli G (2011) Transcriptional regulation of macrophage polarization: enabling diversity with identity. Nat Rev Immunol 11:750–761
50. Ke T, Wu Y, Li L, Liu Y, Yao X, Zhang J et al (2014) Netrin-1 ameliorates myocardial infarction-induced myocardial injury: mechanisms of action in rats and diabetic mice. Hum Gene Ther 25:787–797
51. Li J, Conrad C, Mills TW, Berg NK, Kim B, Ruan W et al (2021) PMN-derived netrin-1 attenuates cardiac ischemia-reperfusion injury via myeloid ADORA2B signaling. J Exp Med. https://doi.org/10.1084/jem.20210008
52. Zhang J, Cai H (2010) Netrin-1 prevents ischemia/reperfusion-induced myocardial infarction via a DCC/ERK1/2/eNOS s1177/NO/DCC feed-forward mechanism. J Mol Cell Cardiol 48:1060–1070
53. Bouhidel JO, Wang P, Siu KL, Li H, Youn JY, Cai H (2015) Netrin-1 improves post-injury cardiac function in vivo via DCC/NO-dependent preservation of mitochondrial integrity, while attenuating autophagy. Biochim Biophys Acta 1852:277–289
54. Westman PC, Lipinski MJ, Luger D, Waksman R, Bonow RO, Wu E et al (2016) Inflammation as a Driver of adverse left ventricular remodeling After acute myocardial infarction. J Am Coll Cardiol 67:2050–2060
55. Li J, Song Y, Jin JY, Li GH, Guo YZ, Yi HY et al (2020) CD226 deletion improves post-infarction healing via modulating macrophage polarization in mice. Theranostics 10:2422–2435
56. Chen Z, Dudek J, Maack C, Hofmann U (2021) Pharmacological inhibition of GLUT1 as a new immunotherapeutic approach after myocardial infarction. Biochem Pharmacol 190:114597

57. Nasser MI, Zhu S, Huang H, Zhao M, Wang B, Ping H et al (2020) Macrophages: first guards in the prevention of cardiovascular diseases. Life Sci 250:117559
58. Greenlee-Wacker MC (2016) Clearance of apoptotic neutrophils and resolution of inflammation. Immunol Rev 273:357–370
59. Garcia RA, Lupisella JA, Ito BR, Hsu MY, Fernando G, Carson NL et al (2021) Selective FPR2 agonism promotes a proresolution macrophage phenotype and improves cardiac structure-function post myocardial infarction. JACC Basic Transl Sci 6:676–689
60. Bao L, Dou G, Tian R, Lv Y, Ding F, Liu S et al (2022) Engineered neutrophil apoptotic bodies ameliorate myocardial infarction by promoting macrophage efferocytosis and inflammation resolution. Bioact Mater 9:183–197
61. Cai X, Shi Y, Dai Y, Wang F, Chen X, Li X (2022) Baicalin clears inflammation by enhancing macrophage efferocytosis via inhibition of RhoA/ROCK signaling pathway and regulating macrophage polarization. Int Immunopharmacol 105:108532
62. DeBerge M, Yeap XY, Dehn S, Zhang S, Grigoryeva L, Misener S et al (2017) MerTK Cleavage on resident cardiac macrophages compromises repair after myocardial ischemia reperfusion injury. Circ Res 121:930–940
63. Marinkovic G, Koenis DS, de Camp L, Jablonowski R, Graber N, de Waard V et al (2020) S100A9 Links inflammation and repair in myocardial infarction. Circ Res 127:664–676
64. Shirakawa K, Endo J, Kataoka M, Katsumata Y, Anzai A, Moriyama H et al (2020) MerTK expression and ERK activation are essential for the functional maturation of Osteopontin-producing reparative macrophages after myocardial infarction. J Am Heart Assoc 9:e17071
65. Vallieres F, Girard D (2017) Mechanism involved in interleukin-21-induced phagocytosis in human monocytes and macrophages. Clin Exp Immunol 187:294–303
66. Ma J, Chen T, Mandelin J, Ceponis A, Miller NE, Hukkanen M et al (2003) Regulation of macrophage activation. Cell Mol Life Sci 60:2334–2346
67. Cai W, Dai X, Chen J, Zhao J, Xu M, Zhang L et al (2019) STAT6/Arg1 promotes microglia/macrophage efferocytosis and inflammation resolution in stroke mice. JCI Insight. https://doi.org/10.1172/jci.insight.131355
68. Shao T, Leung P, Zhang W, Tsuneyama K, Ridgway WM, Young HA et al (2022) Treatment with a JAK1/2 inhibitor ameliorates murine autoimmune cholangitis induced by IFN overexpression. Cell Mol Immunol 19:1130–1140
69. Zhang H, Wang SQ, Hang L, Zhang CF, Wang L, Duan CJ et al (2021) GRP78 facilitates M2 macrophage polarization and tumour progression. Cell Mol Life Sci 78:7709–7732